STUDY OF WIND PRESSURES AND AIR QUALITY AROUND CHILDREN'S HOSPITAL, NATIONAL MEDICAL CENTER

by

F. H. Chaudhry

and

J. E. Cermak

Prepared under contract to

LEO A. DALY COMPANY
Planning Architecture Engineering
Washington, D. C.

Fluid Dynamics and Diffusion Laboratory
Engineering Research Center
Colorado State University
Fort Collins, Colorado 80521

March 1971

CER70-71FHC-JEC55

ABSTRACT

Tests were conducted on a model of the proposed Children's Hospital Facility constructed (1:192 scale) in the Colorado State University Meteorological Wind Tunnel to determine air quality and air pressures around the building. The pressure measurements concentrated on the mean and RMS of the fluctuating pressure at selected locations. Air quality measurements were made by releasing Krypton-85 from specific sources of pollution and sampling it at all the intakes around the building. Data are presented in a manner that these can be directly used to evaluate pressures and air quality. Also, based on these data, recommendations are made on locating the air-conditioning intakes and the sources of pollution.

ACKNOWLEDGMENTS

Many personnel of the Fluid Mechanics Program at Colorado State University have contributed and assisted in this study. The assistance of Mr. S. Sethuraman in pressure experiments and that of Messrs. R. A. Kahawita, S. K. Nayak and S. Putta in diffusion experiments is especially appreciated. Thanks are due to Mr. James E. Garrison for help in preparation of the motion picture and Mr. Ralph Asmus for model construction. Cooperation of Messrs. J. A. Bagala and J. R. McClurg of Leo A. Daly during the course of this investigation is gratefully acknowledged.

TABLE OF CONTENTS

LIST OF TABLES

LIST OF FIGURES

LIST OF FIGURES - (Continued)

LIST OF FIGURES - (Continued)

LIST OF FIGURES - (Continued)

LIST OF SYMBOLS

Symbol	
c	Time mean concentration
C_p	Mean pressure coefficient = $\frac{\overline{P}}{\frac{1}{2}\rho U_{ref}^2}$
$C_{p_{rms}}$	RMS pressure coefficient = $\frac{\sqrt{\overline{p'^2}}}{\frac{1}{2}\rho U_{ref}^2}$
h	Height of the building
I_p	Intensity of pressure fluctuation
K_c	Mean concentration coefficient = $\frac{c}{Q/U_h h^2}$
$\overline{p}$	Mean pressure difference between the local surface pressure and the static pressure in the approaching flow
p'	Fluctuating component of the pressure difference between the location surface pressure and static pressure in the approaching flow
Q	Pollutant release rate
u	Local mean velocity
u_1	Mean velocity at location 1
u_*	Friction velocity = $\sqrt{\tau_o/\rho}$
U_h	Mean velocity at height, h
U_{ref}	Mean velocity at reference height = 100 ft
z	Height
z_o	Roughness length
z_1	Height at position 1
α	Azimuth angle
ρ	Density of air

Symbol	
τ_o	Shear stress at the ground
θ	Deviation from the indicated wind direction positive anti-clockwise.

I. INTRODUCTION

In design of building structures, it is customary to limit the design considerations to the strength of building material vis-a-vis the anticipated loading which can be predicted with confidence. There is another important aspect of design that originates from the need to make the structures safe for the occupants with respect to the immediate environment. This environment is controlled by the meteorological conditions, the distinctive shape of the structure and distribution of the air pollution sources around the building. The environmental design should, then, specifically consider the quality of air being drawn through various proposed intakes around the building, and the distribution of aerodynamic pressure unique for the special shape of the building.

Efforts have been made to universalize the environmental design (Halitsky, 1968) in the same manner as the structural, but such a scheme works only for the elementary geometrical shapes like cubes, cylinders, etc. In actual practice, the building structures do not conform to such geometrical shapes for aesthetic reasons. Often times this departure from simple shapes is necessary due to other more compelling reasons. Thus, many real buildings have projections, set-backs, etc. which introduce significant local perturbations in the flow around them altering greatly the diffusion from a nearby pollution source and the wind pressures. In such cases the data on diffusion and wind pressures for simple shapes are not likely to produce realistic estimates. At the present time, the only approach available for obtaining reliable wind pressure and diffusion data is to study flow around a scale model of the structure placed in a wind tunnel capable of simulating atmospheric motion in the lowest 300 ft.

The purpose of this study is to use the foregoing procedure in the environmental design of the Children's Hospital, National Medical Center, Washington, D. C. There are two distinct features associated with the proposed structure which demand such an investigation. One of these is associated with the irregular geometrical lines of the structure with large glazed areas. Particularly in re-entrant corners mean pressures and pressure fluctuations give cause for concern about glass breakage and leaks around window seals during storms. The second, because of the use for which the building is intended, is the need to make certain that air drawn into the building is uncontaminated by air exhausted from the building or from neighboring pollution sources.

A 1:192 scale model of the hospital building was placed in the Colorado State University meteorological wind tunnel. Direct measurements of mean pressures and root-mean-square values of pressure fluctuations were made using pressure transducers. Also, concentrations of tracer released at significant locations were obtained at nearly all the proposed intake points for air conditioning. These data were obtained for four wind directions.

This investigation is significant in that it constitutes a part of the overall design of the hospital. The concentration data provide a picture of the quality of air that is available around the proposed structure and fixes the position of high pollutant concentration areas with respect to the different sources of pollution. This information can be useful in locating the air conditioning intakes and in determining the optimum location of pollution sources such as air conditioning exhausts and parking area exhaust parts. The wind pressure data

provide useful information for selection of window glass, development of specifications for seals and design of the reception entrance area.

The basis of simulation, experimental arrangement and the results are discussed in detail in the body of the report.

II. SIMULATION OF FLOW

In order that the wind-tunnel test results correspond to those expected in the field, the air flow around the model should be similar to the prototype flow. The conditions for such a similarity are usually found in the equations of motion for a given flow. Cermak et al. (1966), Halitsky (1968), Cermak and Arya (1970) and many others have discussed a variety of modeling problems and their similarity requirements. It is generally agreed that, in the case of a neutral* atmosphere, dynamic similarity would be achieved if the model satisfies the following criteria:

(1) Geometrical similarity

(2) Reynolds number $(\frac{UL}{\nu})$ similarity

(3) Boundary condition similarity.

Geometrical similarity requires that all the components of the structure be scaled in the same proportion as components of the proposed building. The actual maximum scale possible is limited by width of the wind-tunnel test section. The meteorological wind tunnel has a cross section of 6 ft x 6 ft. In order to avoid interference by walls of the wind tunnel, the model should occupy no more than the center 3 ft of the tunnel floor. As the model is to be studied for various wind directions, the maximum model dimension is represented by a diagonal which is about 600 ft in extent. Thus a scale of 1:200 satisfies the space requirement. A scale of 1:192 was, however, found to be more convenient for model construction as all the floor plan drawings for the building were made to this scale.

---

*No temperature stratification

Using the same scale for the vertical dimensions yields a model height of about 0.5 ft. The maximum blockage presented by the model at this scale is about 4% -- a value sufficiently small to cause no concern about distortion of the flow. Moreover, this blockage was considerably reduced when the wind-tunnel roof was raised to produce zero pressure gradient over the model.

For a sharp-edged structure, Reynolds number equality is not essential and the flow patterns are similar if a critical lower limit of the Reynolds number is exceeded. The drag coefficient for a sharp-edged body becomes a constant above a Reynolds number of about 3×10^3. Also according to Golden (1961) as quoted by Halitsky, the diffusion patterns around sharp-edged structures are invariant for Reynolds numbers greater than 11,000. As both the model and prototype are placed in air flow, this diffusion critical Reynolds number corresponds to UL = 2 ft /sec. The proposed Children's Hospital building is about a hundred feet high, therefore, the Reynolds numbers in the prototype would be above the critical if the wind speed is greater than $\frac{1}{50}$ ft/sec which is nearly always true. The wind-tunnel air speeds used are 30 ft/sec and 50 ft/sec so that the Reynolds number in the wind tunnel is also greater than the critical. Thus both the model and the prototype are in the class of flows which are independent of Reynolds number and the fact that the model Reynolds number is approximately 100 times less than the prototype value does not invalidate the flow similarity.

Boundary condition similarity requires that the approach flows be similar in the model and prototype. Because of the long test section it was possible to create mean velocity and turbulence profiles which have characteristics typical of an urban atmosphere. This was

facilitated by modeling the terrain surrounding the building with trees. The urban geometry up to 1 mile upwind from the building was modelled in the wind tunnel by placing street blocks in the same orientation found in the prototype.

In view of the preceding discussion and the past experience, it can be said with some confidence that the flow over the proposed Children's Hospital building in its selected location was portrayed in the model and that the results can be used for design purposes on the full-scale structure. The flow conditions investigated in this study correspond to strong winds and as such its results are not expected to apply in calm conditions when the dynamics of the exhausts assumes primary importance.

III. EXPERIMENTAL ARRANGEMENT

Wind Tunnel

Model tests were conducted in the meteorological wind tunnel at the Fluid Dynamics and Diffusion Laboratory of Colorado State University. The tunnel, specifically designed to study fluid phenomena of the atmosphere, has a 6 ft square by 90 ft long test section with an adjustable ceiling to provide a zero pressure gradient over the model (see Fig. 1). This tunnel was operated as a closed circuit. A 6 ft length of test-section floor at the leading edge was roughened with ½ in. gravel to increase the boundary-layer thickness. The model was located on the wind-tunnel floor about 80 ft from the test section entrance. At this location the turbulent boundary layer simulating the atmospheric boundary layer was about 30 in. thick or about five times the model height. This permits excellent simulation of the atmospheric shear flow to be encountered by the completed structure. Wind speeds in the wind tunnel can be varied from 1 ft/sec to 100 ft/sec. As discussed earlier, because of the sharp-edged geometry of the structure, the wind speed can be varied over a wide range without affecting the local flow characteristics.

Model

The model of the Children's Hospital consisted of the proposed building, the neighboring structures of the Washington Hospital, the topography of surrounding terrain and an approximate representation of the city block extending to about a mile upwind from the hospital. All the features were constructed to a scale of 1:192. The terrain was made of styrofoam sheets which were cut to match the ground contours

and then glued together. The entire model was mounted on plywood sheets such that the nearby topography could be moved to face wind from different directions. Other buildings of the National Medical Center were also modeled by styrofoam blocks and were fixed on to the terrain. To model the city blocks, bricks (2¼ in. x 3½ in. x 7½ in.) were laid out in random heights but with due regard to alignment of city streets.

The Children's Hospital building proper was constructed from ½ in. thick "Lucite" sheets. The outside features of each floor were machine cut to render a strong model. The model was built to proper dimensions according to the details provided by Leo A. Daly. As the floor plans differed from each other, outside detail of nearly each floor was constructed separately. Each component has machine cut bevelled ends. The pieces were cemented together to create the model shown in Fig. 1 which is both sufficiently attractive for display and rugged to serve the aerodynamic modeling function.

Fifty-nine piezometric taps 1/16 in. in diameter were drilled through the model surface at all levels as shown in Figs. 2 to 4. Their locations were selected to give adequate coverage of critical points near the sharp-edged corners. Nearly eighty diffusion sampling taps 1/8 in. in diameter were also placed at the proposed air-conditioning intakes. Figures 5 to 8 show these sampling points on the building elevations. Flexible plastic tubings from each pressure and sampling tap were taken out through the wind-tunnel floor. The building model was placed on a turntable to permit continuous rotation about a vertical axis. Figure 9 presents some views of the model in the wind tunnel. Another simplified model of Children's Hospital was made from plywood to simulate the flow through open areas around the building

at the level V-1. Special care was taken to model the details at this level, e.g., the openings on the east, south and west sides; openings in floor levels V-1 and V-2; openings connecting the levels V-2 and V-3 with the parking ramps, etc.

Wind and Pressure Measurement

A pitot-static tube was used to measure the upstream mean velocity profile and set the mean wind speeds. Pitot-static tube output was monitored through M.K.S. electronic pressure meter. This instrument was also used to measure mean pressures on the model building walls. All the pressure and velocity measurements were made at a speed of 50 ft/sec to ensure a favorable signal to noise ratio. Five "Statham" differential pressure transducers (Model PM283) were employed to measure the fluctuating component of the pressure. The reference ports of the "Statham" pressure transducers were connected through a manifold to the static pressure tap of the pitot tube. The other side of each transducer was connected to a separate pressure tap around the building. With this arrangement, the transducer measured the fluctuations of the pressure between the local surface pressure and the static pressure in the free stream. The root-mean-square (RMS) value of the fluctuating pressure was measured through a DISA True RMS meter (Model 55 D35). A Tektronix storage oscilloscope (Type 562) and a Hewlett-Packard digital voltmeter (Model 3440 A) were used to calibrate the transducers and to check the output signal during the experiment. Figure 10 shows a block diagram of the pressure measuring instruments.

Turbulence measurements in the approaching flow were made with a hot-wire anemometer. The anemometer output was connected to the DISA RMS meter and the RMS was recorded on a Moseley X-Y recorder (Type 135).

Flow Visualization

The initial phase of data collection was the visualization of flow around the building. Smoke was introduced at significant locations over the model to identify the problem areas on the building requiring detailed measurements. The smoke was produced by passing compressed air through a container of titanium-tetrachloride located outside the wind tunnel. A color 16 mm motion picture of the visualized flow was produced to provide a permanent record of its characteristics.

Air Quality Sampling

Four different sources of pollution were considered in this study viz.,

(1) Car parking area exhausts (Fig. 11)

(2) Roof stacks (Fig. 12)

(3) Contagious diseases laboratory exhaust (NE corner) (Fig. 5)

(4) Proposed power room stacks (Fig. 11).

Krypton-85 was used for the tracer gas and was introduced into the model system through a flow meter. For each pollution source, the quality of air at various air-conditioning intakes around the building was determined by sampling the tracer gas-air mixture and measuring the concentration of Kr-85 in the mixture. The details of the sampling system are sketched in Fig. 13. Samples were drawn from the wind tunnel through 1/8 in. I.D. flexible tubing and collected in the glass bottle by displacement over water. This arrangement enabled 25 samples to be obtained at the same time for one release and, thus, conserves the radioactive Kr-85. In order to collect the samples, negative air pressure is created in the reservoir and the ball valve is opened. Each sample was transferred into a cylindrical jacket around a Geiger-Mueller (G.M.) tube by a

reverse process. The jacket was then filled with water and pressure applied to air in the reservoir forced the sample from a collector bottle to the jacket. The volume of the jacket was exactly equal to that of the sample collected. Four jacketed G.M. tubes were used to facilitate transfer and analysis. Each G.M. tube was calibrated against a gas of known concentration. The samples after transfer to G.M. tube jackets were counted by a Nuclear-Chicago ultrascaler.

IV. TEST RESULTS AND THEIR APPLICATION

Test Program

To meet the objectives set forth for this investigation, the following data were obtained by flow visualization and direct measurement:

1. Motion pictures of flow made visible by introduction of smoke.
2. Characteristics of flow approaching the model structure.
3. Characteristics of winds at level V-1.
4. Mean pressures and root-mean-square values of pressure fluctuations on exterior surface of the building.
5. Air quality measurements.

The test conditions are indicated in the detailed discussion of each type of the data. In the wind tunnel, the wind velocities were set by monitoring the free stream, i.e., velocities outside the boundary layer. As it is not practicable to measure its equivalent in the field, the pressure and air quality data are presented taking approach wind velocity at a height equivalent to the top of the building ($\simeq$100 ft) as the reference velocity. Also, wind direction is defined as the direction from which the wind originates.

Test Results: Flow Visualization

Two series of experiments were conducted to visualize the detailed structure of flow around the building. The first such series covered observations of the dispersion patterns of smoke introduced through each individual source of pollution. These observations were made for four wind directions, viz., north, north-west, west and south. A color motion picture was taken for those tests which were considered significant in determining the quality of air surrounding the hospital. Of special

interest is the character of flow on the north side of the building for north and south winds and in the set-backs at levels C and D on the east and west sides. The north-side characteristics were revealed by smoke releases through proposed underground parking area exhausts at ground level situated near the middle of the north wall. For south winds, the smoke is driven against the north wall whereas for the north wind, it is removed and diffused. Both of these results could be derived by appeal to the existing knowledge on details of flow around a sharp-edged obstacle (see, for example, Halitsky, 1963).

When the wind comes from the south, a secondary flow is set up in the opposite direction behind the building. The return flow is strongest at the axis of the toroidal vortex pair and produces a stagnation region near the bottom of the north face of the building. The flow is upward and radially outward from this region. The parking area exhaust under consideration happens to be at the axis of the secondary flow and thus the effluent is carried to the north wall and spread radially on this face. In the case of north wind, the existing Washington Hospital Center has a profound effect on the flow around the Children's Hospital building. If there were no buildings upwind, the north face of the proposed building would have a radial flow outward from the stagnation region and smoke would be carried to the north wall. The presence of buildings upwind from the hospital, however, introduces a set of vortices in the space between them. The secondary flow at the ground is again opposite to the main stream and away from the north face. The flow along this face is inward to a pseudo-stagnation region.

The other interesting observation of smoke was made for the releases from the roof sources near the east and west sides (Fig. 12). These sources are situated on the corner of a recess on each side. For north and south winds, the smoke released from the sources upwind from the recess tends to spiral into the recess. These observations are completely corroborated by the detailed concentration measurements which are presented later in this chapter.

The second series of visualization tests was made on the plywood model. The smoke source was placed at the level V-1 and then its transport studied for south and west winds. These are the only relevant directions as there is no opening on the north side of level V-1. For a south wind, there was observed a weak flow out on the east and west sides which was overpowered by the primary flow. The flow through the east opening at level V-1 due to the west wind was observed to be strong enough to advance against the opposite secondary flow near the ground but could not cross the cavity. Thus the flow through the openings at level V-1 is not expected to interfere with the general pattern of flow.

Test Results: Approach Flow

Although the flow characteristics in the immediate vicinity of the structure are dominated by its particular geometry, the mean velocity profile of the approaching flow controls the shape of the wake boundary and secondary flow in the cavity. In view of this, approach flow was conditioned by modeling the topographical features up to about a mile from the Children's Hospital. The resulting velocity profile, for a south wind, 1,000 ft upwind from the building, is shown in Fig. 14. Its characteristics are investigated in Figs. 15 and 16. A logarithmic

law is known to better fit the velocity profile close to the surface in neutral conditions, i.e.,

$$\frac{u}{u_*} = \frac{1}{k} \ln \frac{z}{z_o} .$$

Figure 15 shows a plot of the velocity vs height on a semi-log paper. The roughness length z_o in the model corresponds to about 1 ft in the prototype. This value of z_o is typical of the open area having isolated trees (Jenson, 1958). The National Medical Center does not have any densely populated area within half a mile on all sides, especially so for the south wind. This gives support to the velocity profile produced over the model. For the north wind, the flow upwind from the Children's Hospital is conditioned also by the Washington Hospital Center complex. Another representation, which is commonly used, is the power law form of velocity profile, viz.,

$$\frac{u}{u_1} = \left(\frac{z}{z_1}\right)^{\alpha}$$

where u_1 is the velocity at height z_1 and the exponent α is the indicator of surface roughness for neutral flow. For the approach flow in the wind tunnel (Fig. 16) α is about 0.4 which is again typical of a thinly populated area. A value of 1/7 for α corresponds to a smooth surface.

The turbulence profile of the approach flow is shown in Fig. 17. The intensity of turbulence varies from 50% near the surface to about 20% at the building height. These figures compare well with the observation made on Fort Wayne, Indiana by Hilst and Bowne (1966).

Test Results: "Winds" at Level V-1

Detailed measurements of wind and turbulence were made at a number of locations at the V-1 which are indicated in Fig. 18. This was done to examine if an undue gustiness could prevail in this parking area due to the openings on the west, south and east sides. The data are presented in Table I. It is noted that the flow both in the mean and the fluctuation is damped in the parking area. The wind velocity through the openings on the east and west sides is of the order of one-third the reference wind (i.e., the wind velocity at the building height) for the south winds. The wind will be gusty at the entrance to the pipe bridge on the south side. If the average wind is, say, 3 mph, the gusts may go up to 8 mph. Similarly, the wind will be gusty in some of the ramps leading to the parking area, but the winds will be generally weaker.

Test Results: Surface Pressure

The local mean pressures $\overline{P}$ measured with respect to ambient pressure can be expressed in the form of non-dimensional pressure coefficient C_p (to facilitate its use for design purposes) as,

$$C_p = \frac{\overline{P}}{\frac{1}{2}\rho U_{ref}^2}$$

where ρ is the density of air and U_{ref}, the reference wind velocity. Table II presents the non-dimensional pressure at all the pressure taps for different wind directions. A practical statistic of the random pressure fluctuations is its root-mean-square (RMS) value. The RMS pressure p_{rms} can also be non-dimensionalized either to express it as a coefficient, i.e.,

$$C_{p_{rms}} = \frac{\sqrt{\overline{p'^2}}}{\frac{1}{2}\rho U_{ref}^2}$$

or as pressure fluctuation intensity

$$I_p = \frac{\sqrt{\overline{p'^2}}}{\overline{p}} \times 100$$

The pressure fluctuation data for selected positions is presented in both the forms in Table III. At places, the pressure fluctuation intensity is very high indicating either that the mean pressures are very weak or that the fluctuations are strong. In Table IV is presented the variation of pressure fluctuation on five pressure taps as a function of the azimuth angle α. These data are also illustrated in Fig. 19 for three taps at level C. It will be noted the maximum fluctuations occur in a wind at right angles to (or slightly different from it) the face of the building on which the pressure taps are situated. For this reason, the pressure fluctuation data in Table III are obtained for the azimuth of $\pm 6°$.

Test Results: Air Quality

The concentration measurements around the building, such as pressure data, must also be represented in the form of a suitable non-dimensional concentration coefficient K_c which is universal to both the model and the prototype. A useful form for K_c is

$$K_c = \frac{c\, U_h\, h^2}{Q}$$

where c is the concentration (say, mg/ft^3), Q, the rate of release of pollutant (mg/sec) and U_h the velocity (ft/sec) at building height h (100 ft in the prototype). All the concentration data observed in the wind tunnel have been rendered into this non-dimensional form. These K_c values are to be presented for a number of intakes at four

levels for three different types of pollution sources which are tested for four wind directions. Also the building plan and the position of intakes is different at each level. In such a situation, it is best to consider each level and each source separately. Thus, each building level has been developed open and the K_c values plotted against the intake positions for various wind directions on one sheet of graph paper. In Figs. 20 through 31 is displayed all the information on the distribution of pollutants obtained in this study. As the fourth category of pollution, namely, the proposed powereroom stack exhaust escaped the building completely, no graph on it is presented.

An examination of these figures reveals the positions of the maximum concentration around the building for a given source. Underground parking area exhausts cause maximum concentrations at the north and southeast intakes. The roof stacks exhaust is found to be least diluted at intakes located in the dents in levels C and D on the east and west sides. The contagious diseases laboratory exhaust delivers most of its pollution to the intakes around the northeast corner. The observations on the first two types of sources match remarkably with the visualization results described earlier.

Applications

Practical application of the quantitative results is attempted in this section. As all these results have been presented in a form which is independent of the model to prototype scale, the required information can be obtained simply by substituting the prototype data into the results of this study.

Example: What are the maximum positive and negative pressures to which a window glass at level 'C' is subjected at S.T.P. in an approach

wind velocity of 40 miles/hr at the height of the building? Also find the maximum fluctuating pressure RMS value and its relation to the mean.

A glance through mean pressure data in Table II gives

$$[C_p]_{\text{max. pos.}} = .715 \quad \text{(on pressure tap CSP 7 for westerly wind)}$$

$$[C_p]_{\text{max. neg.}} = -.915 \quad \text{(on pressure tap CEP 2 for southerly wind)}$$

By definition: $C_p = \dfrac{\bar{p}}{\frac{1}{2}\rho U_{ref}^2}$ $\therefore$ $\bar{P} = \frac{1}{2}\rho C_p U_{ref}^2$

with, $U_{ref} = 40$ mph $= 58.7$ ft/sec

$\rho_{air} = .002378$ slugs/ft^3

$$\text{Maximum positive mean pressure} = \frac{1}{2} \times (.715) \times .002378 \times (58.7)^2$$

$$= 2.93 \text{ lb/ft}^2$$

$$\text{Maximum negative mean pressure} = \frac{1}{2} \times (.915) \times .002378 \times (58.7)^2$$

$$= 3.75 \text{ lb/ft}^2.$$

Also from Table III, the maximum fluctuating pressure coefficient at level 'C' is

$$C_{p_{rms}} = \frac{\text{RMS pressure}}{\frac{1}{2}\rho U_{ref}^2} = .596 \quad \text{(on CWP 6 for southerly wind)}$$

$$\therefore \text{ RMS pressure} = \frac{1}{2}(.596) \times .002378 \times (58.7)^2$$

$$= 2.44 \text{ lb/ft}^2.$$

From the same table, the RMS of fluctuating pressure is twice the mean pressure.

Example: Evaluate the quality of air around the building especially in respect of pollutants released through underground parking exhausts,

namely, carbon monoxide, unburnt hydrocarbons and nitrogen oxides in an approaching wind of 10 mph at the building height.

The first step in this evaluation is to estimate, Q, the amount of each pollutant being released around the building. The parking area has a total capacity of accommodating 1,000 cars but only those cars would be emitting exhaust which are in transit. There is no direct way of calculating the maximum number of cars that would have their engines running at a given instant. We assume, therefore, that no more than 50 cars are either idling or accelerating between 0 and 10 mph at any instant. Concentrations of CO and hydrocarbon emissions are maximum in the engine idle mode and decrease as the engine speed is increased outside of the idle range. NO_x concentrations are on the low side for lower speeds (see Stern, 1968). Average composition of car exhausts in transit in the parking area can be taken to be (averaged over 0-10 mph range from the curves in Fig. 3, page 59 of Stern, 1968)

CO	4.46×10^{-3} lb/ft^3 of exhaust gas
Hydrocarbons	2000 ppm
NO_x	1000 ppm.

If an average car exhausts at a rate of 20 ft^3/min (see Maga and Kinosian, 1968), the amount of each pollutant released by 50 cars is

$$Q = \left\{ \begin{array}{ll} \text{CO} & 4.46 \times 10^{-3} \times 20 \times 50/60 = 0.074 \text{ lb/sec} \\ \text{Hydrocarbons} & 2000 \times 20 \times 50/60 = 3.34 \times 10^4 \text{ ppm ft}^3\text{/sec} \\ NO_x & 1000 \times 20 \times 50/60 = 1.67 \times 10^4 \text{ ppm ft}^3\text{/sec} \end{array} \right\}.$$

With U_h = 10 mph = 14.7 ft/sec and h = 100 ft,

the reference concentrations are

$$\frac{Q}{U_h\ h^2} = \left\{ \begin{array}{ll} CO & 5.05 \times 10^{-7}\ lb/ft^3 = 8.1\ mg/m^3 \\ \text{Hydrocarbons} & 0.228\ ppm \\ NO_x & 0.114\ ppm \end{array} \right\} .$$

Now if the air quality standards for CO, hydrocarbons and NO_x are known, we can find a K_c value corresponding to such standards for each pollutant and compare the observed K_c values with permissible K_c. Let us assume the following standards:

Pollutant	Permissible Standard c_{per}	Permissible $K_c = \frac{c_{per}}{Q/U_h h^2}$
CO	60 mg/m for 1 hour	60/8.1 = 7.4
Hydrocarbons	0.5 ppm " "	0.5/0.228 = 2.2
NO_x	0.2 ppm " "	0.2/0.114 = 1.76

These assumed permissible K_c values are imposed on the appropriate data and are shown in Figs. 32-35. It appears that it might be possible to satisfy CO standards more easily than the permissible standards for hydrocarbons and NO_x.

Example: What would be the carbon monoxide concentration at the intake AWD1 in Fig. 6 due to the parking area exhausts (500,000 ft^3/min) during a north-west wind of 10 miles per hour if its concentration at the exhaust is 100 ppm?

The non-dimensional concentration at AWD1 is obtained from the parking area exhaust data for level 'A' in Fig. 20 for the given wind as

$$K_c = \frac{c}{Q/U_h\ h^2} = 1.75$$

or $c_{AWD1} = 1.75\ \ Q/U_h\ h^2$.

From the given data,

$Q = 100$ ppm x 500,000 $ft^3/min = 5 \times 10^7$ ppm ft^3/min

$U_h = \frac{10 \times 5280}{60}$ ft/min = 880 ft/min

$h = 100$ ft.

Hence,

$$c_{AWD1} = \frac{1.75 \times 5 \times 10^7}{880 \times 10^4} \text{ ppm}$$

$$\cong 10 \text{ ppm}$$

These examples merely illustrate the practical application of the results of this study. Their procedure, however, must be repeated with more reliable information on air quality standards and specific design data.

V. CONCLUSIONS AND RECOMMENDATIONS

Information on the expected interaction between the proposed Children's Hospital, National Medical Center and its immediate environment is obtained through wind tunnel tests on its model. The pressure measurements made on the model can be directly used for design purposes. The quality of air around the proposed structure may be evaluated from the reduced data on concentrations. It is recommended that the example of application of air quality data should be repeated with more reliable information on air quality standards in the Washington area and more accurate description of sources of pollution. Such evaluation should be made for all types of pollution.

Based on the visualization results and diffusion data, some parking area exhausts should be considered for relocation. As a general rule, no such exhausts (for example, exhaust no. 4 in Fig. 11) should be centrally placed on any side of the building. The preferable location for the ground sources is where the effluent can escape the reverse secondary flow in order to minimize chances of undiluted pollutants being brought to the intakes. The reverse flow occurs behind the building and in the immediate vicinity of its sides. Hence, the sources should be located, as far as possible, away from the building along diagonals radiating from the building corners (see Fig. 11). However, if the exhaust locations are fixed, it is recommended that non-operating windows should be provided on the north side at the points AND2, AND3, BND3, BND4, CND5, CND6, CND7, DND2 and DND3 in Fig. 5. If possible the intakes in the recesses on the east and west side at levels 'C & D', namely, CED2, CWD4, DED2 and DWD3 (see Figs. 6 and 8) should be avoided.

The proposed design of power-room stacks is shown to be satisfactory as the building completely escapes the effluents. The parking area at level 'V-1' is not found to be windy as suspected. The winds are found to be quite gusty, however, in the mini park.

REFERENCES

Cermak, J. E., et al. (1966), "Simulation of Atmospheric Motion by Wind Tunnel Flows," Colorado State University, Engineering Research Center Report No. CER66JEC-VAS-EJP-GJB-HC-RNM-SI-17.

Cermak, J. E. and Arya, S. P. S. (1970), "Problems of Atmospheric Shear Flows and Their Laboratory Simulation," Boundary Layer Meteorology 1, pp. 40-60.

Golden, J. (1961), "Scale Model Techniques," M.A. Thesis, Department of Meteorology and Oceanography, New York University.

Halitsky, J. (1963), "Gas Diffusion near Buildings," Transactions Am. So. Heating, Refrig. Air-Cond. Eng. 69, pp. 464-484.

Halitsky, J. (1968), "Gas Diffusion near Buildings," Meteorology and Atomic Energy, 1968, published by U.S. Atomic Energy Commission, pp. 221-255.

Hilst, G. R. and Bowne, N. E. (1966), "A Study of the Diffusion of Aerosols Released from Aerial Line Sources Upwind of an Urban Complex," Final Report, Contract No. DA42-007-AMC-38(R), to Dugway Proving Ground, The Travellers Research Center, Inc., Hartford, Connecticut.

Jenson, M. (1958), "The Model-Law for Phenomena in Natural Wind," Ingenioeren, 2, pp. 121-128.

Maga, J. A. and Kinosian, J. R. (1966), "Motor Vehicle Emission Standards - Present and Future," Paper 660104 presented at SAE Automotive Engineering Congress, Detroit, January 1966.

Stern, A. C. (1968), "Air Pollution," Vol. III, Academic Press.

TABLES

TABLE I WIND SPEED AND TURBULENCE AT LEVEL 'V-1'

U_{ref} = velocity of approaching wind at the height of the building (100 ft)

Wind Direction	Station*	$\frac{\text{Mean Wind}}{U_{ref}}$	$\frac{\text{Max. Gusts}}{\text{Mean Wind}}$	Turbulence Intensity $= \frac{\text{Fluct. RMS}}{\text{Mean Wind}} \times 100$ %
South	1	.42	1.15	10
	2	.41	1.13	10
	3	.32	1.19	20
	4	.27	1.13	24
	5	.34	1.32	23
	6	.32	1.32	31
	7	.22	1.42	51
	8	.30	1.48	42
	9	.32	1.42	34
	10	.09	2.14	72
	11	.20	1.44	42
	12	.07	2.61	65
	13	.23	1.35	16
	14	.21	1.24	25
	15	.35	1.28	22
	16	.29	1.87	21
	17	.20	1.51	42
	18	.38	1.80	39
	19	.16	2.39	61
West	20	.37	1.09	8
	21	.48	1.12	8

*See Fig. 18 for station location.

TABLE II MEAN PRESSURE COEFFICIENT C_p FOR VARIOUS WIND DIRECTIONS

Pressure Tap* \ Direction of wind	Northerly		Southerly		Westerly		North-westerly
	$\theta^{\dagger} = +6°$	$\theta^{\dagger} = -6°$	$\theta = +6°$	$\theta = -6°$	$\theta = +6°$	$\theta = -6°$	$\theta = 0°$
ANP1	+.035	+.104	-.132	-.216	-.388	-.358	-.061
ASP1	-.253	-.269	+.180	+.687	-.180	+.180	-.865
ASP2	-.238	-.254	+.299	+.373	-.327	-.061	-.654
ASP3	-.096	-.134	+.538	+.456	-.061	+.122	-.208
ASP4	-.134	-.157	+.477	+.456	+.015	+.134	-.299
ASP5	-.167	-.203	+.269	+.400	-.299	-.327	-.538
AEP1	-.142	-.172	-.477	-.586	-.256	-.284	-.299
AEP2	-.150	-.086	-.119	-.373	-.208	-.226	-.327
AEP3	-.715	-.538	-.208	-.251	-.192	-.289	-.358
AWP1	-.104	-.180	-.388	-.400	+.596	+.388	+.299
AWP2	-.162	-.388	-.446	-.487	+.477	+.388	+.074
AWP3	-.238	-.269	-.477	-.586	+.299	+.322	-.418
AWP4	-.299	-.327	-.015	+.586	+.299	+.358	-.775
AWP5	-.248	-.248	+.180	+.329	+.342	+.383	-.446
BSP1	-.243	-.264	+.134	+.629	-.327	+.150	-.775
BSP2	-.208	-.203	+.299	+.358	-.446	-.401	-.657

† θ is defined as below

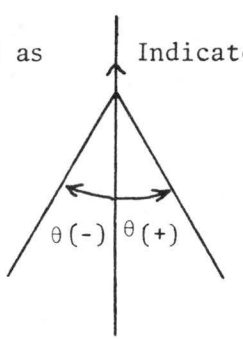

TABLE II MEAN PRESSURE COEFFICIENT C_p FOR VARIOUS WIND DIRECTIONS - Continued

Pressure Tap* \ Direction of wind	Northerly		Southerly		Westerly		North-westerly
	$\theta = +6°$	$\theta = -6°$	$\theta = +6°$	$\theta = -6°$	$\theta = +6°$	$\theta = -6°$	$\theta = 0°$
BEP1	-.142	-.139	-.446	-.629	-.253	-.269	-.238
BEP2	-.745	-.626	-.208	-.256	-.188	-.276	-.327
BWP1	-.035	-.216	-.238	-.287	+.180	-.129	+.477
BWP2	-.208	-.256	-.299	-.299	+.418	+.269	+.388
BWP3	-.208	-.507	-.388	-.429	+.553	+.507	+.150
BWP4	-.233	-.281	-.446	-.601	+.373	+.388	-.299
CSP1	-.231	-.243	+.060	+.456	-.715	-.446	-.657
CSP2	-.231	-.226	+.269	+.373	+.030	.000	-.388
CSP3	-.165	-.162	+.568	+.472	-.122	+.061	-.299
CSP4	-.129	-.149	+.418	+.358	-.487	-.403	-.388
CEP1	-.190	-.216	-.180	-.429	-.446	-.609	-.358
CEP2	-.190	-.231	-.834	-.915	-.253	-.243	-.269
CEP3	-.089	+.327	-.238	-.314	-.233	-.284	-.269
CEP4	-.198	-.048	-.061	-.314	-.231	-.281	-.477
CEP5	-.226	-.208	-.299	-.216	-.253	-.269	-.388
CWP1	-.162	-.271	-.314	-.358	+.208	+.223	-.015
CWP2	-.216	-.269	-.299	-.335	-.099	+.193	-.208
CWP3	-.134	-.233	-.358	-.423	+.373	+.269	-.030
CWP4	+.104	-.134	-.284	-.314	-.193	-.071	+.568
CWP5	-.066	-	-.388	-.400	+.327	+.208	+.150
CWP6	-.215	-.264	-.806	-.299	+.269	+.492	-.388
CWP7	-.226	-.215	+.269	-	+.388	+.715	-.418
CWP9	-.142	-.137	+.418	-	+.538	+.507	-.208

TABLE II MEAN PRESSURE COEFFICIENT C_p FOR VARIOUS WIND DIRECTIONS - Continued

Pressure Tap* \ Direction of wind	Northerly		Southerly		Westerly		North-westerly
	$\theta = +6°$	$\theta = -6°$	$\theta = +6°$	$\theta = -6°$	$\theta = +6°$	$\theta = -6°$	$\theta = 0°$
DNP1	-.129	-.015	-.150	-.172	-.223	-.243	-.030
DNP2	-.030	+.119	-.193	-.195	-.715	-.687	+.446
DSP1	-.226	-.238	+.180	+.342	-.507	-.538	-.745
DSP2	-.208	-.221	+.388	+.456	-.299	-.418	-.865
DSP3	-.157	-.172	+.687	+.629	-.358	-.253	-.269
DSP4	-.139	-.162	+.299	+.358	-.243	-.216	-.715
DEP1	-.167	-.187	-.089	-.299	-.446	-.507	-.269
DEP2	-.215	-.226	-.865	-.256	-.243	-.253	-.269
DEP3	-.084	+.203	-.538	-.358	-.254	-.269	-.238
DEP4	-.248	-.157	-.208	-.372	-.223	-.274	-.596
DEP5	-.251	-.142	+.299	-.200	-.208	-.276	-.538
DWP1	-.162	-.274	-.418	-.444	+.446	+.477	+.073
DWP2	-.198	-.281	-.269	-.271	-.208	-.150	-.150
DWP3	-.238	-.314	-.477	-.477	+.327	.314	-.238
DWP4	+.165	-.089	-.418	-.388	-.183	-.104	+.715
DWP5	-.137	-.373	-.388	-.373	+.365	+.327	+.418
DWP6	-.193	-.233	-.806	-.629	+.487	+.626	-.180
DWP7	-.256	-.253	-.089	-	+.388	+.657	-.477
DWP8	-.231	-.223	+.180	-	+.446	+.626	-.327
DWP9	-.150	-.142	+.269	-	+.507	+.657	-.327

*See Figs. 2-4 for position of pressure taps.

TABLE III $C_{p_{rms}}$ FOR VARIOUS WIND DIRECTIONS

Direction of wind - - - Southerly

$\theta = +6°$

Pressure Tap	$C_{p_{rms}}$	Fluctuation Intensity %
ASP2	.137	46
ASP5	.180	67
AEP3	.071	34
BWP1	.071	30
BWP4	.150	33
CNP1	.010	-
CWP5	.474	122
CWP6	.525	65
CWP7	.150	56
CWP8	.241	-
CWP9	.185	44
DSP1	.281	156
DEP1	.261	294
DEP2	.335	39
DEP3	.114	21
DWP6	.281	35

$\theta = -6°$

Pressure Tap	$C_{p_{rms}}$	Fluctuation Intensity %
ASP3	.124	27
AEP1	.076	13
BEP1	.233	37
BEP2	.094	28
CEP1	.360	84
CEP2	.302	33
CEP3	.106	34
CEP4	.106	34
CWP6	.596	199
CWP7	.147	-

TABLE III $C_{p_{rms}}$ FOR VARIOUS WIND DIRECTIONS - Continued

Direction of wind - - - Northerly

$\theta = + 6°$

Pressure Tap	$C_{p_{rms}}$	Fluctuation Intensity %
ANP1	.099	278
ASP1	.074	29
AEP1	.071	50
AEP2	.094	63
AEP3	.243	34
AWP1	.124	12
AWP2	.112	69
AWP3	.079	33
AWP4	.071	24
AWP5	.063	25
BSP1	.074	30
BEP1	.079	55
BEP2	.388	52
BWP1	.172	485
BWP2	.281	135
BWP3	.152	73
BWP4	.079	34
CSP2	.079	34
CEP4	.081	41
CEP5	.104	46
CWP1	.099	48
CWP2	.251	116
CWP3	.101	75
CWP4	.241	231
CWP5	.185	281
CWP6	.106	49
CWP7	.081	39
CWP9	.073	52
DNP1	.188	148
DNP2	.013	41
DSP1	.076	34
DSP2	.074	35
DSP3	.071	45
DSP4	.086	62
DEP1	.129	77
DEP2	.076	35
DEP3	.200	239

$\theta = - 6°$

Pressure Tap	$C_{p_{rms}}$	Fluctuation Intensity %
ASP1	.180	67
ASP2	.231	90
ASP3	.063	47
ASP4	.099	63
ASP5	.058	29
AEP3	.063	12
BSP1	.256	97
BSP2	.172	85
BEP1	.071	51
BEP2	.071	11
CSP1	.388	332
CSP2	.276	122
CSP3	.226	139
CSP4	.304	203
CEP3	.106	32
CEP5	.099	205
DSP4	.304	187
DEP3	.124	61
DEP4	.063	40
DEP5	.094	66

TABLE III $C_{p_{rms}}$ FOR VARIOUS WIND DIRECTIONS - Continued

Direction of wind - - - Northerly

$\theta = +6°$ (Cont'd)

Pressure Tap	$C_{p_{rms}}$	Fluctuation Intensity %
DEP4	.106	43
DEP5	.096	38
DWP1	.117	67
DWP2	.101	51
DWP3	.132	55
DWP4	.281	171
DWP5	.274	200
DWP6	.089	46
DWP8	.094	41

TABLE III $C_{p_{rms}}$ FOR VARIOUS WIND DIRECTIONS - Continued

Direction of wind - - - Westerly

$\theta = + 6°$

Pressure Tap	$C_{p_{rms}}$	Fluctuation Intensity %
ANP1	.079	20
ASP2	.172	53
AEP1	.056	22
AWP2	.109	23
BEP2	.061	32
BWP3	.147	27
CNP1	.008	--
CSP1	.373	52
CSP2	.345	1133
CSP3	.256	210
CSP4	.289	59
CEP1	.152	34
CEP2	.071	28
CEP3	.106	47
CEP4	.074	32
CWP1	.203	57
CWP2	.302	90
CWP3	.208	49
CWP4	.200	64
CWP5	.165	41
CWP6	.193	64
CWP7	.175	--
CWP8	.183	--
DNP1	.074	33
DNP2	.185	26
DSP2	.335	112
DEP1	.150	33
DEP2	.081	33
DWP2	.335	161
DWP4	.200	110

$\theta = - 6°$

Pressure Tap	$C_{p_{rms}}$	Fluctuation Intensity %
ASP1	.180	100
ASP2	.231	379
ASP3	.063	48
ASP4	.099	74
ASP5	.058	18
AEP3	.063	22
BSP1	.256	171
BSP2	.172	43
BEP1	.071	26
BEP2	.071	26
CSP1	.388	87
CSP2	.276	$\approx \infty$
CSP3	.226	370
CSP4	.304	75
CEP3	.106	37
CEP5	.099	37
DSP4	.304	141
DEP3	.124	46
DEP4	.063	23
DEP5	.094	34

TABLE III $C_{p_{rms}}$ FOR VARIOUS WIND DIRECTIONS - Continued

Direction of wind - - - North Westerly

$\theta = 0°$

Pressure Tap	$C_{p_{rms}}$	Fluctuation Intensity %
ANP1	.132	22
ASP1	.226	26
ASP2	.160	24
ASP3	.074	35
ASP4	.066	22
AEP1	.081	27
AEP2	.068	21
AEP3	.086	24
AWP1	.200	67
AWP2	.137	186
AWP3	.101	24
AWP4	.167	22
AWP5	.167	37
BSP1	.137	18
BSP2	.150	23
BEP1	.074	31
BEP2	.094	29
BWP1	.172	36
BWP2	.251	65
BWP3	.226	151
BWP4	.142	47
CSP2	.093	24
CEP4	.101	21
CWP1	.106	700
CWP2	.106	51
CWP3	.183	600
CWP4	.274	48
CWP5	.325	217
CWP6	.127	33
CWP7	.134	32
CWP9	.117	56
DNP1	.165	541
DNP2	.390	87
DSP1	.099	13
DSP2	.150	17
DSP3	.132	49
DSP4	.137	19
DEP1	.071	26
DEP2	.096	36
DEP3	.132	55
DEP4	.104	17
DEP5	.109	20
DWP2	.132	88
DWP3	.208	87

TABLE IV VARIATION OF $C_{P_{rms}}$ WITH AZIMUTH ANGLE, α
FOR TYPICAL PRESSURE TAPS

Azimuth Angle, α \ Pressure Tap	CSP1	BEP2	CEP1	CWP6	DWP5	Remarks
0	.251	.066	.360	.596	.109	Southerly
10	.233	.066	.274	.431	.134	Wind
20	.188	.063	.210	.261	.132	
30	.157	.071	.157	.175	.134	
40	.137	.081	.160	.134	.119	
50	.117	.101	.203	.109	.099	
60	.106	.137	.226	.089	.079	
70	.109	.172	.233	.086	.071	
80	.086	.221	.259	.074	.068	
90	.078	.233	.304	.066	.066	Easterly
100	.071	.172	.312	.071	.068	Wind
110	.089	.160	.274	.071	.071	
120	.094	.170	.203	.074	.084	
130	.079	.180	.188	.081	.094	
140	.074	.254	.165	.086	.096	
150	.066	.281	.137	.081	.119	
160	.071	.339	.109	.086	.205	
170	.079	.347	.094	.101	.256	
180	.081	.294	.079	.109	.248	Northerly
190	.094	.246	.081	.109	.218	Wind
200	.081	.155	.079	.094	.292	
210	.086	.127	.082	.109	.377	
220	.101	.086	.086	.122	.299	
230	.114	.071	.081	.157	.317	
240	.137	.063	.079	.200	.256	
250	.172	.061	.079	.200	.261	
260	.281	.053	.114	.193	.274	
270	.345	.056	.150	.185	.231	Westerly
280	.352	.051	.172	.170	.213	Wind
290	.352	.061	.190	.157	.200	
300	.259	.061	.188	.165	.162	
310	.195	.074	.190	.200	.124	
320	.208	.091	.216	.238	.104	
330	.266	.096	.274	.281	.086	
340	.233	.084	.327	.350	.079	
350	.233	.071	.345	.520	.086	

FIGURES

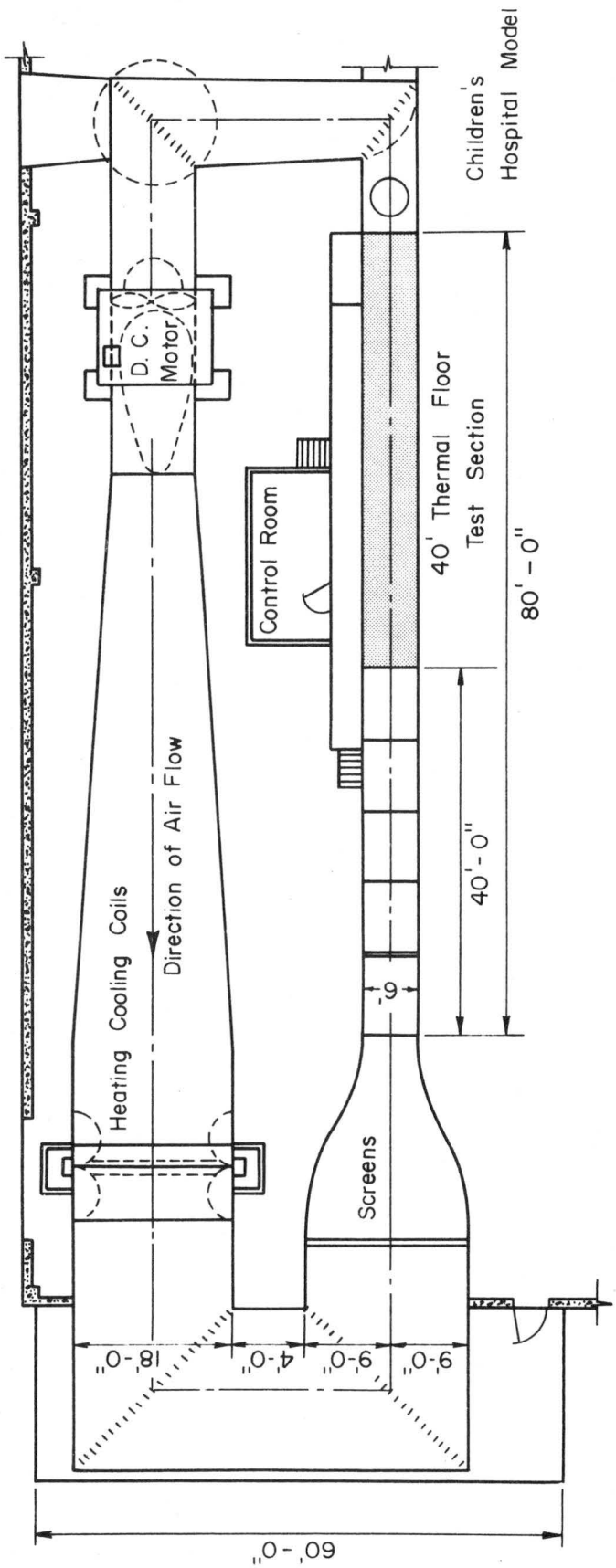

Fig. 1. Meteorological wind tunnel.

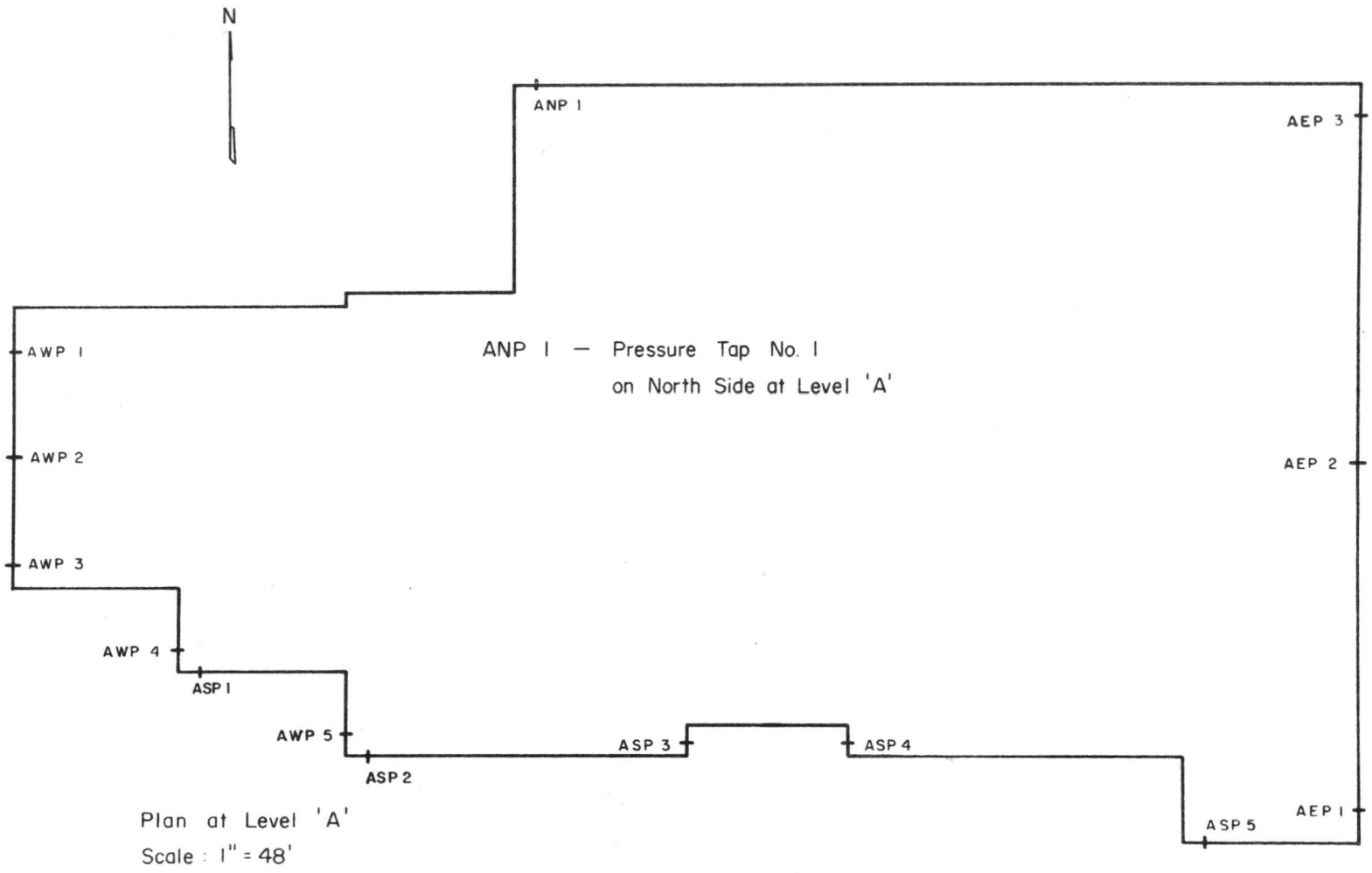

Fig. 2. Position of piezometric taps at level 'A'.

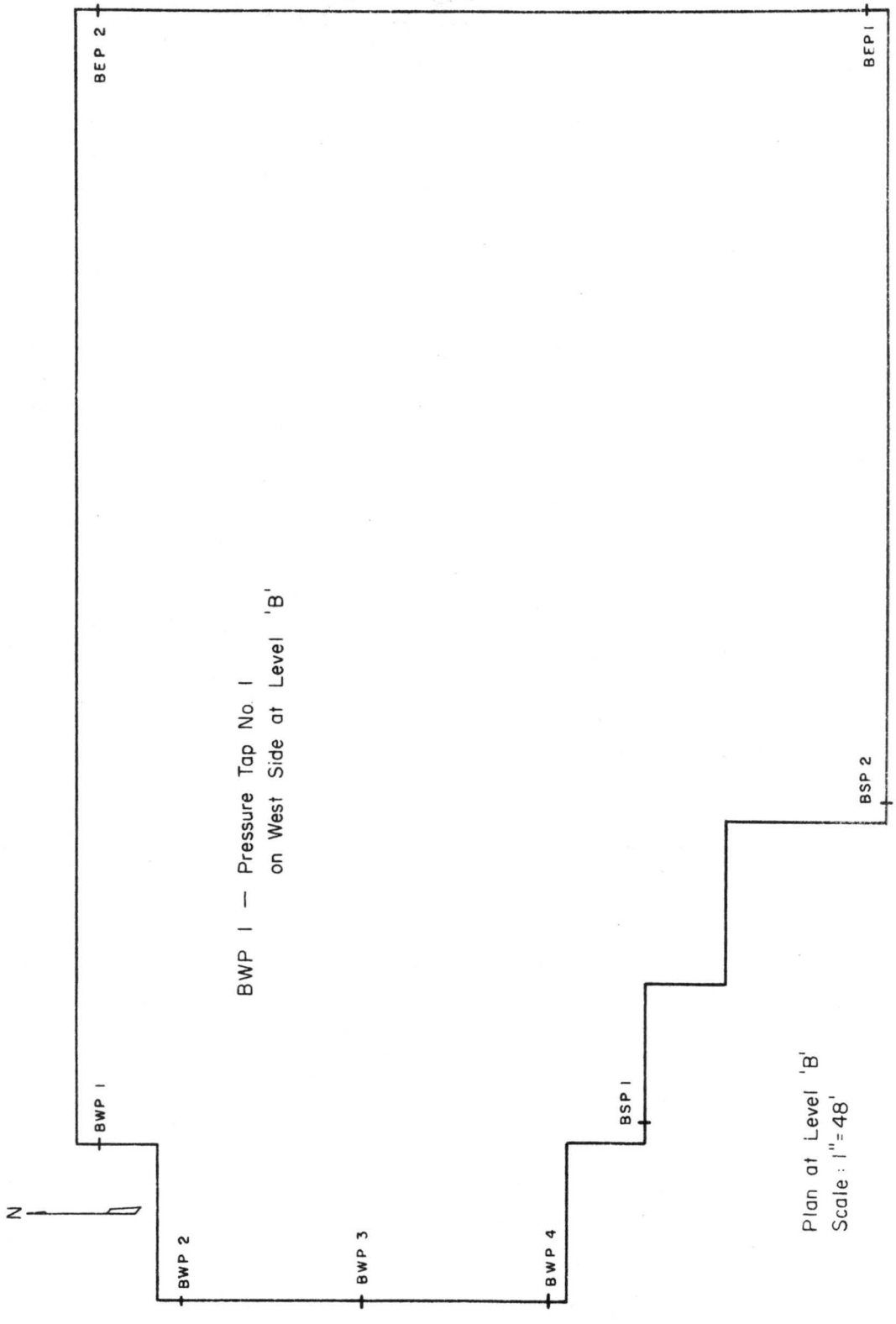

Fig. 3. Position of piezometric taps at level 'B'.

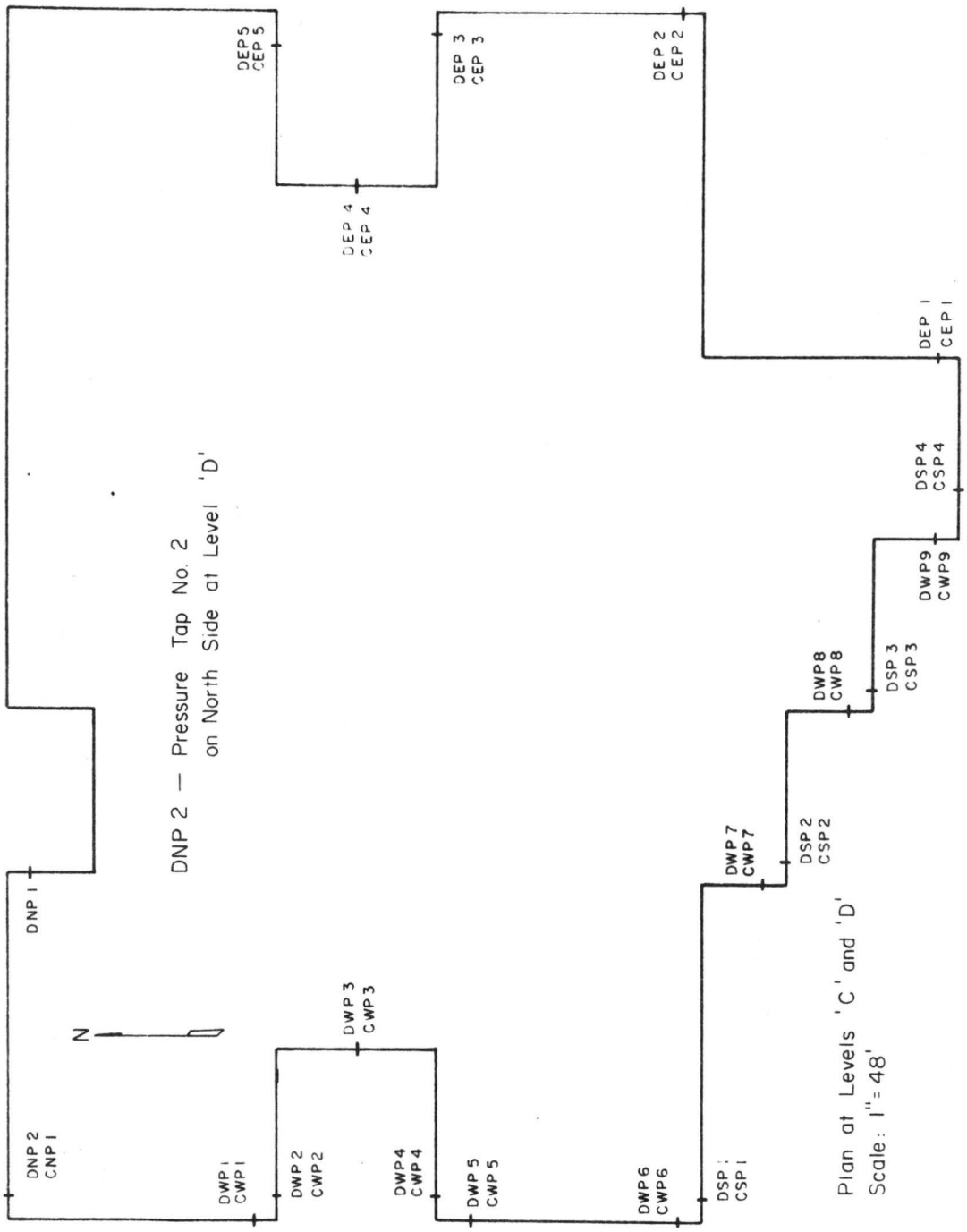

Fig. 4. Position of piezometric taps at level 'C'.

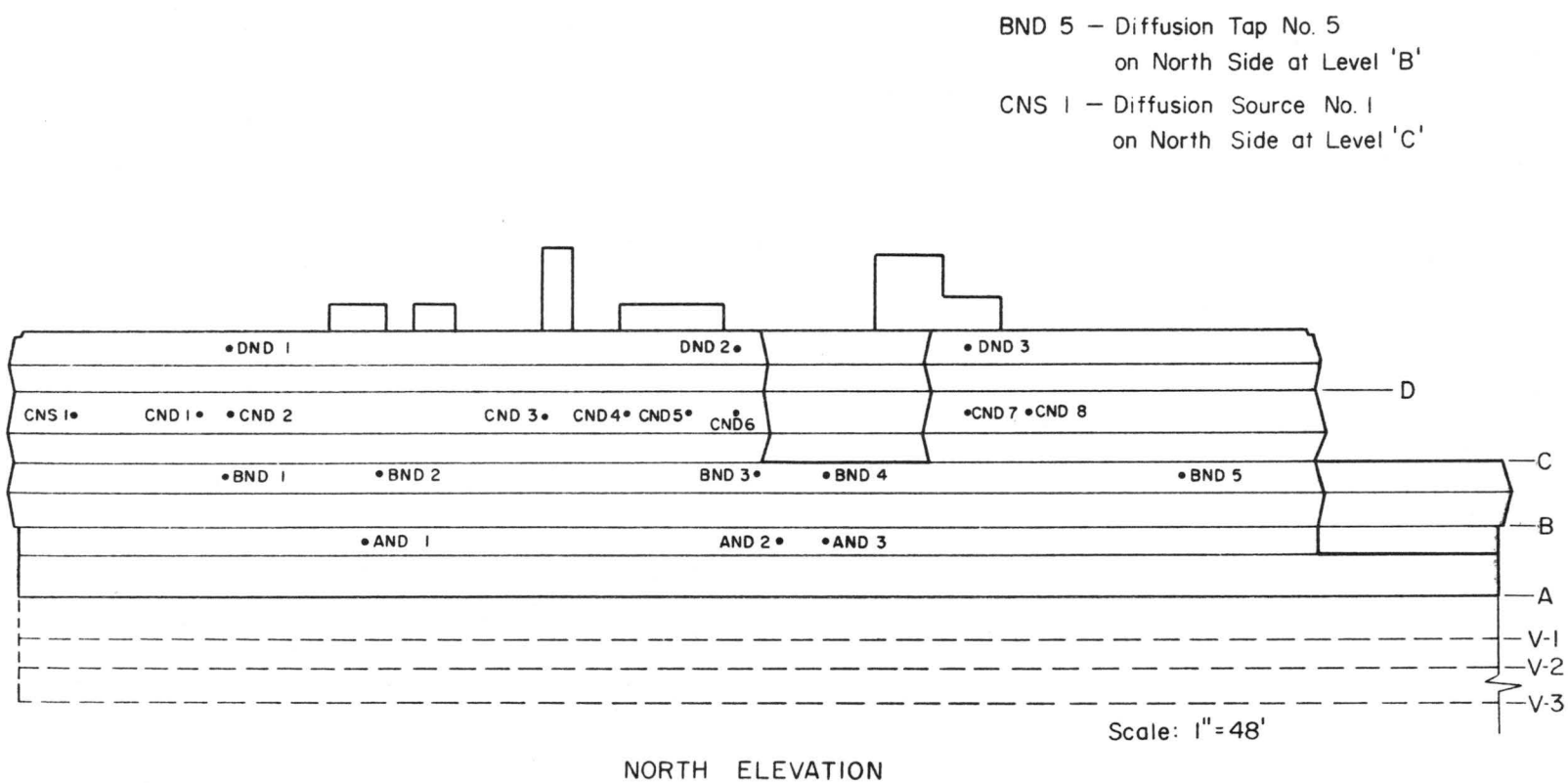

NORTH ELEVATION

Fig. 5. Position of diffusion sampling taps on the north side.

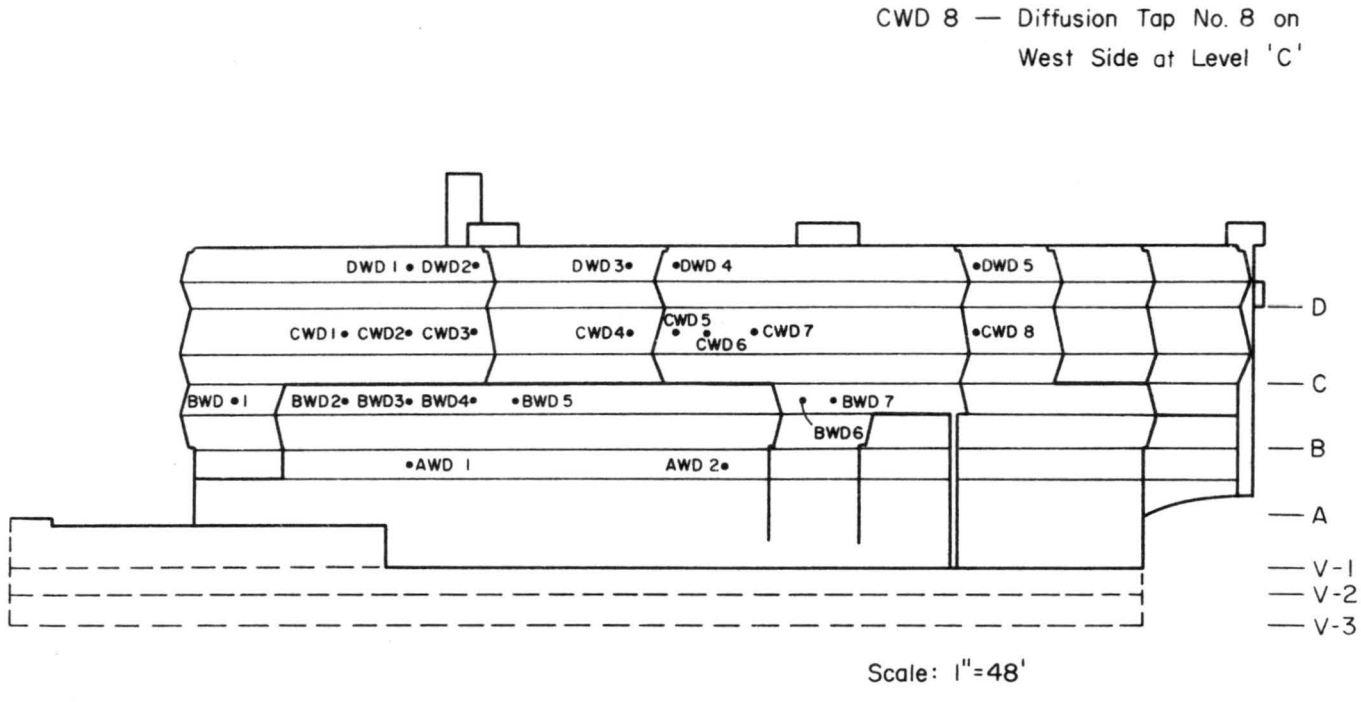

Fig. 6. Position of diffusion sampling taps on the west side.

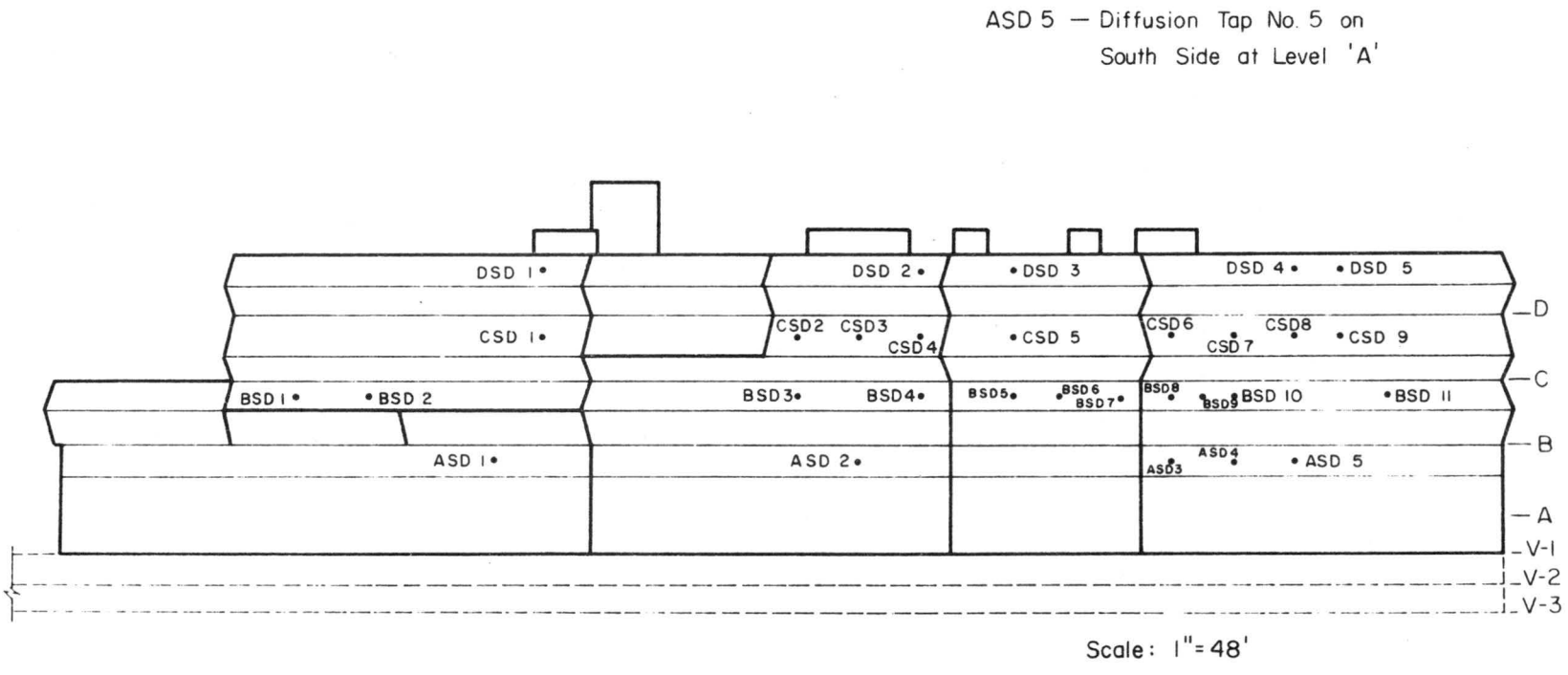

SOUTH ELEVATION

Fig. 7. Position of diffusion sampling taps on the south side.

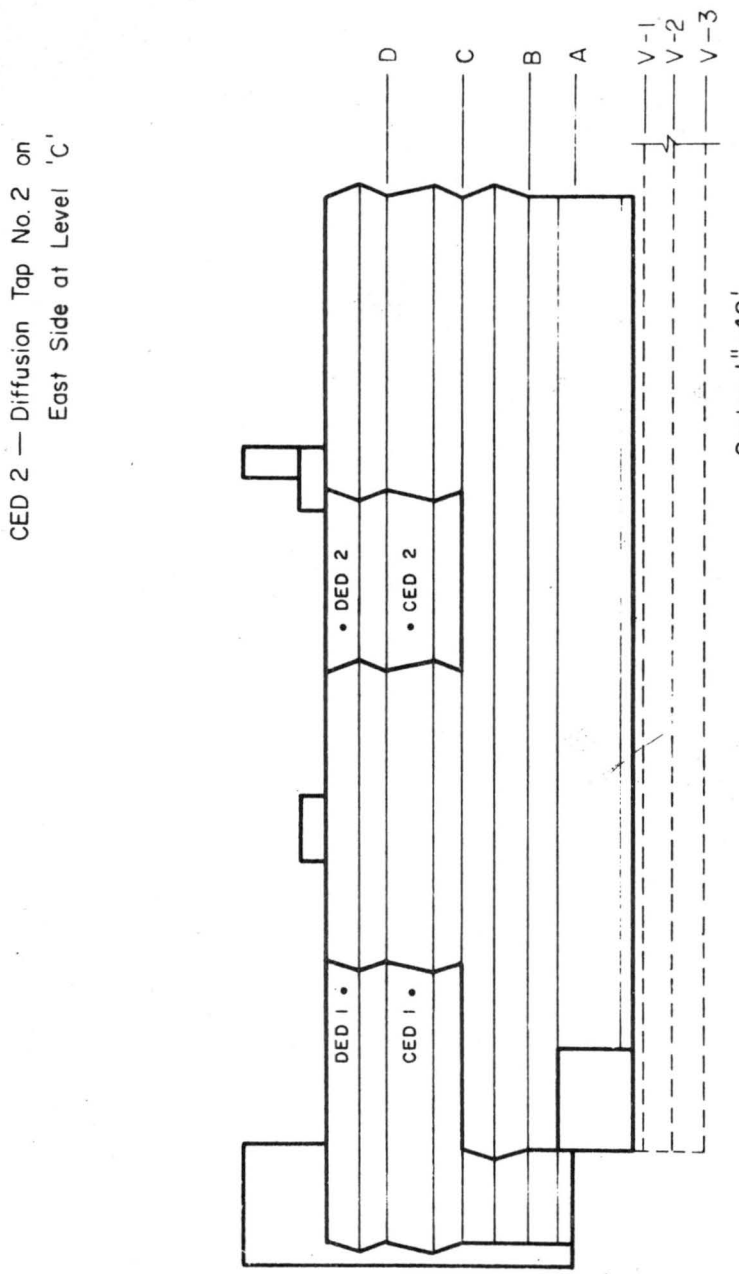

Fig. 8. Position of diffusion sampling taps on the east side.

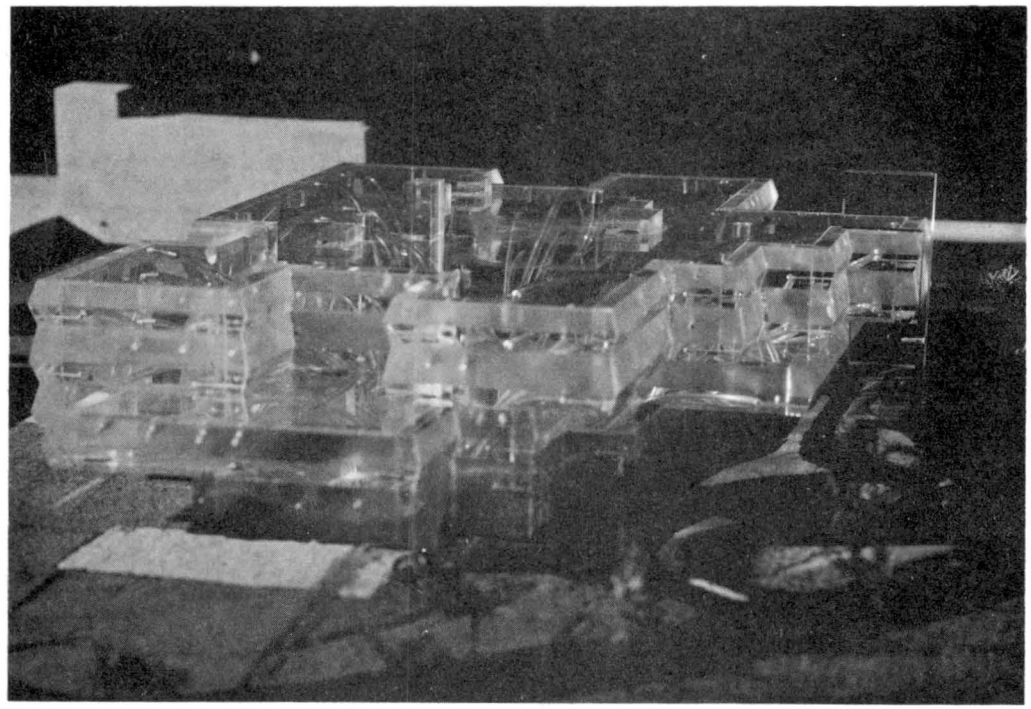

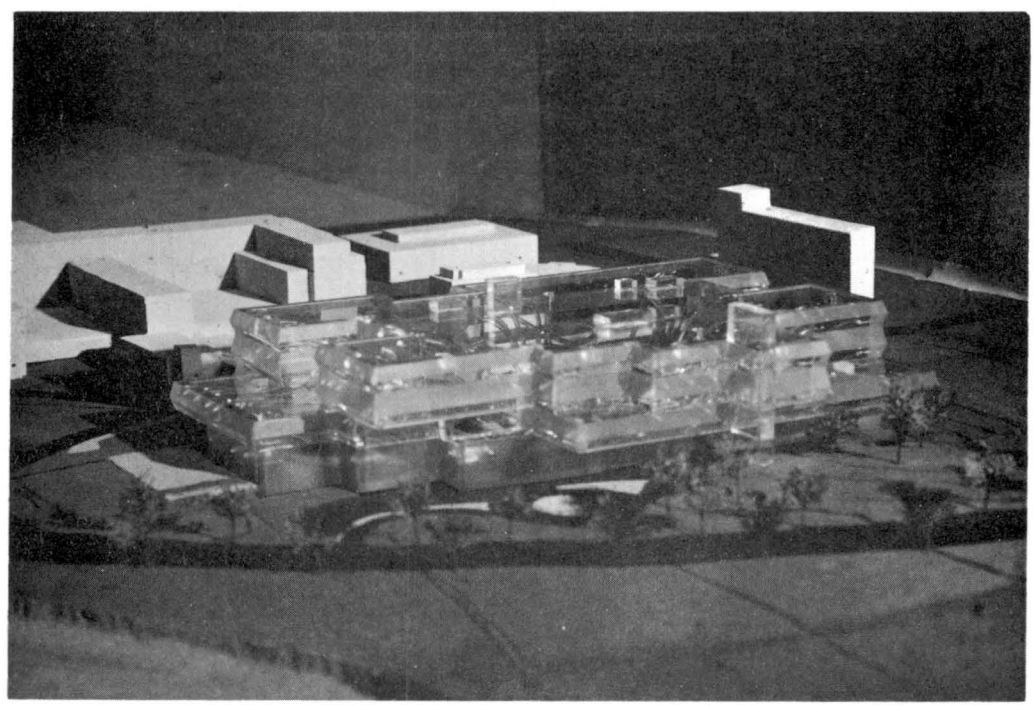

Fig. 9. Model of Children's Hospital facility and the National Medical Center.

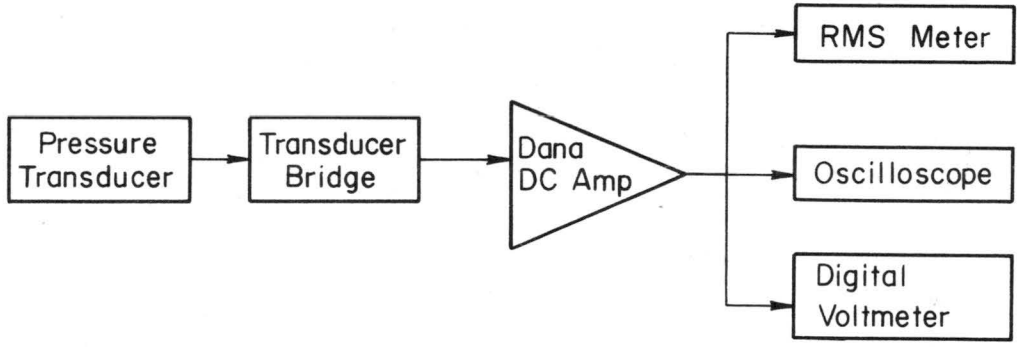

Fig. 10. Block diagram of instruments used in RMS pressure measurement.

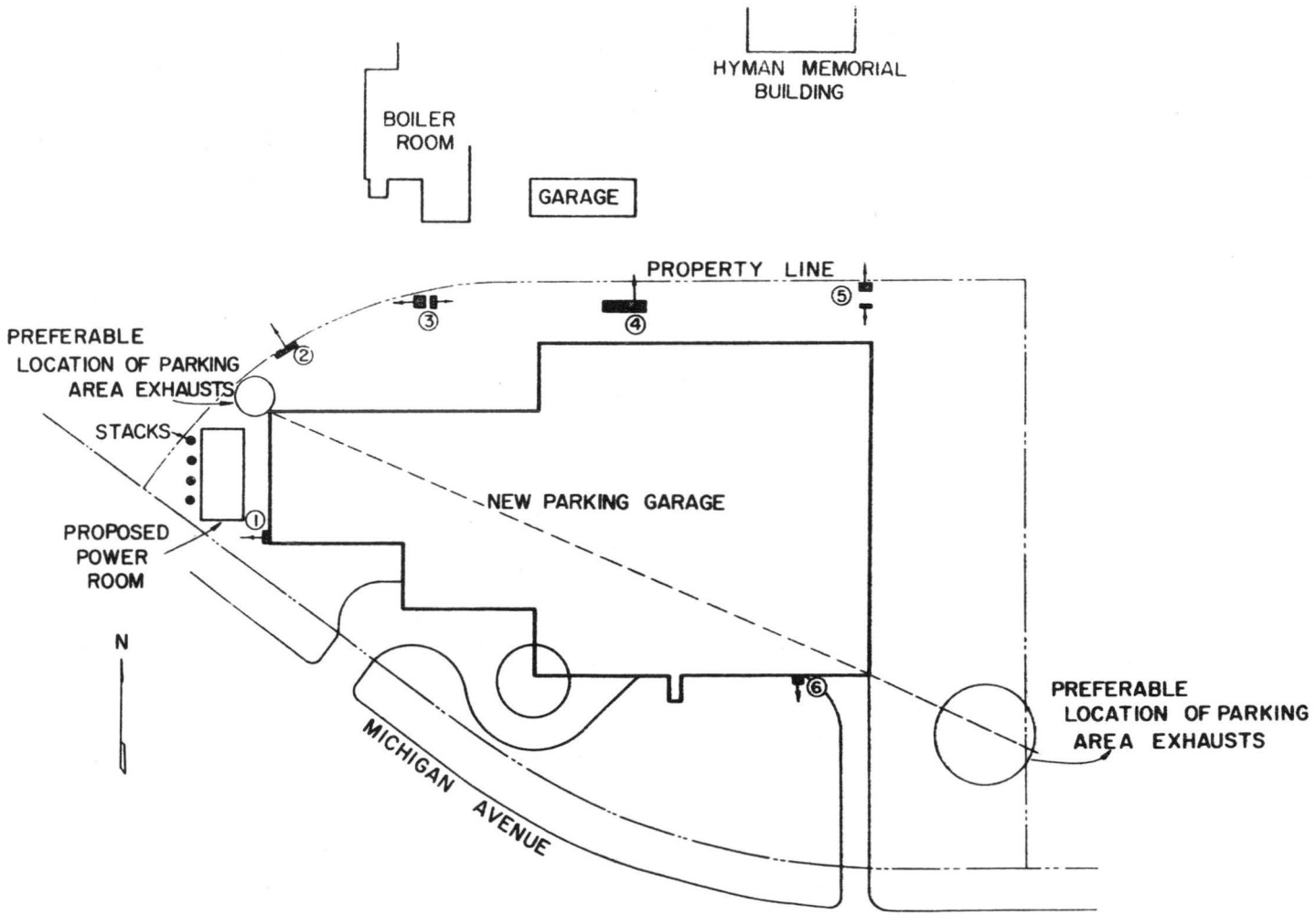

Fig. 11. Site plan showing underground parking area exhausts.

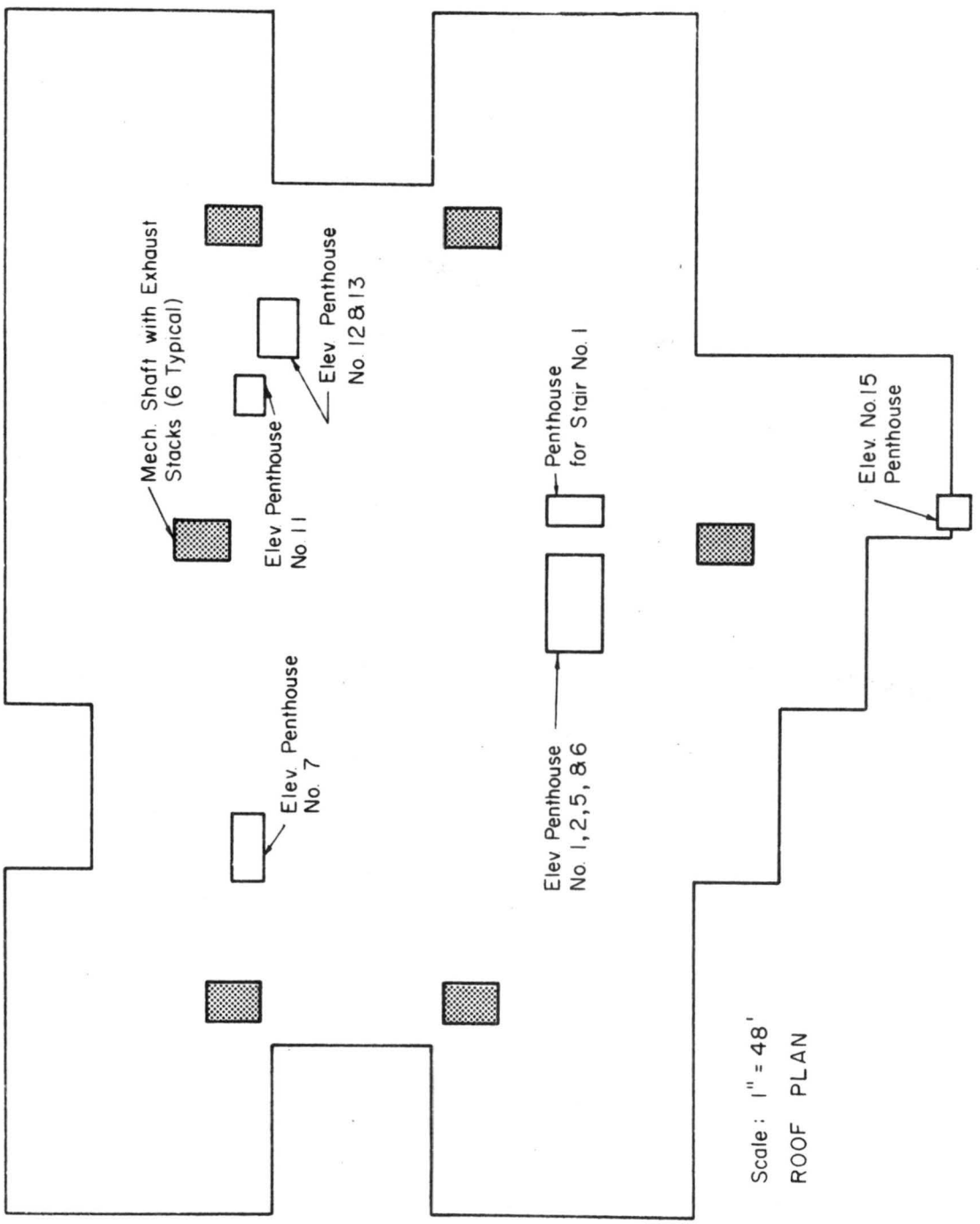

Fig. 12. Roof plan showing roof stacks.

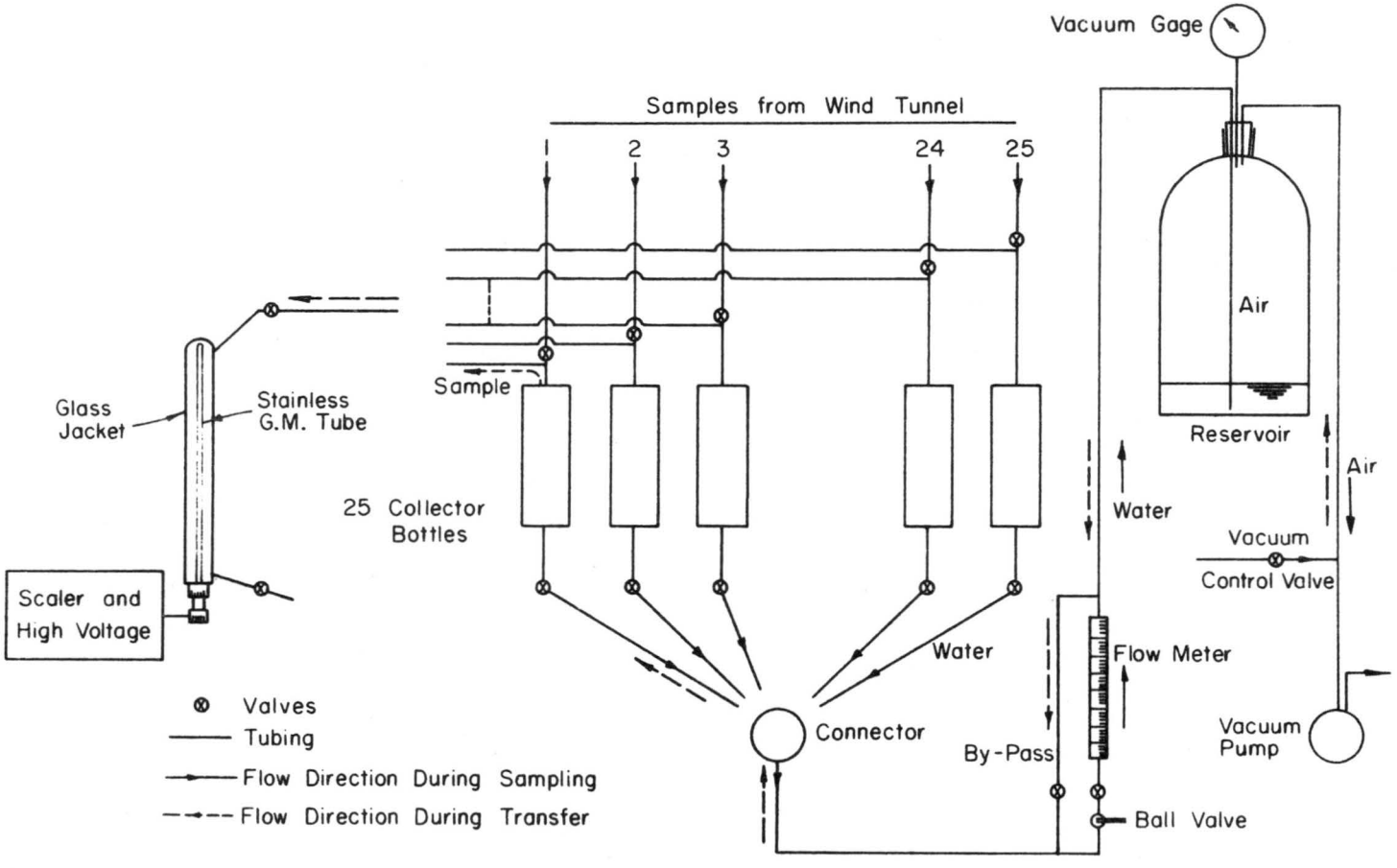

Fig. 13. Diffusion sampling and detection system.

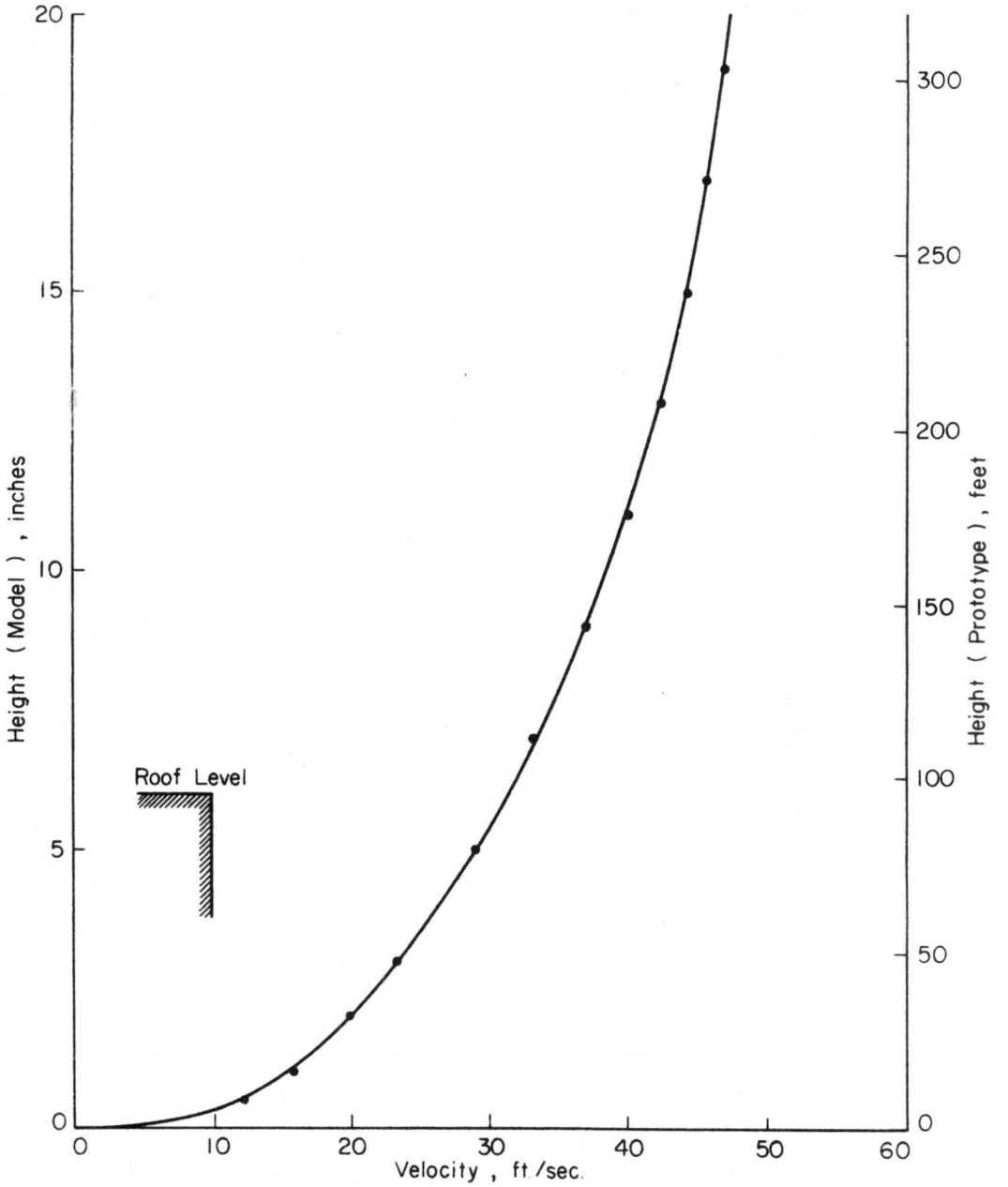

Fig. 14. Approach flow velocity profile at a distance equivalent to 1000 ft upwind from Children's Hospital facility.

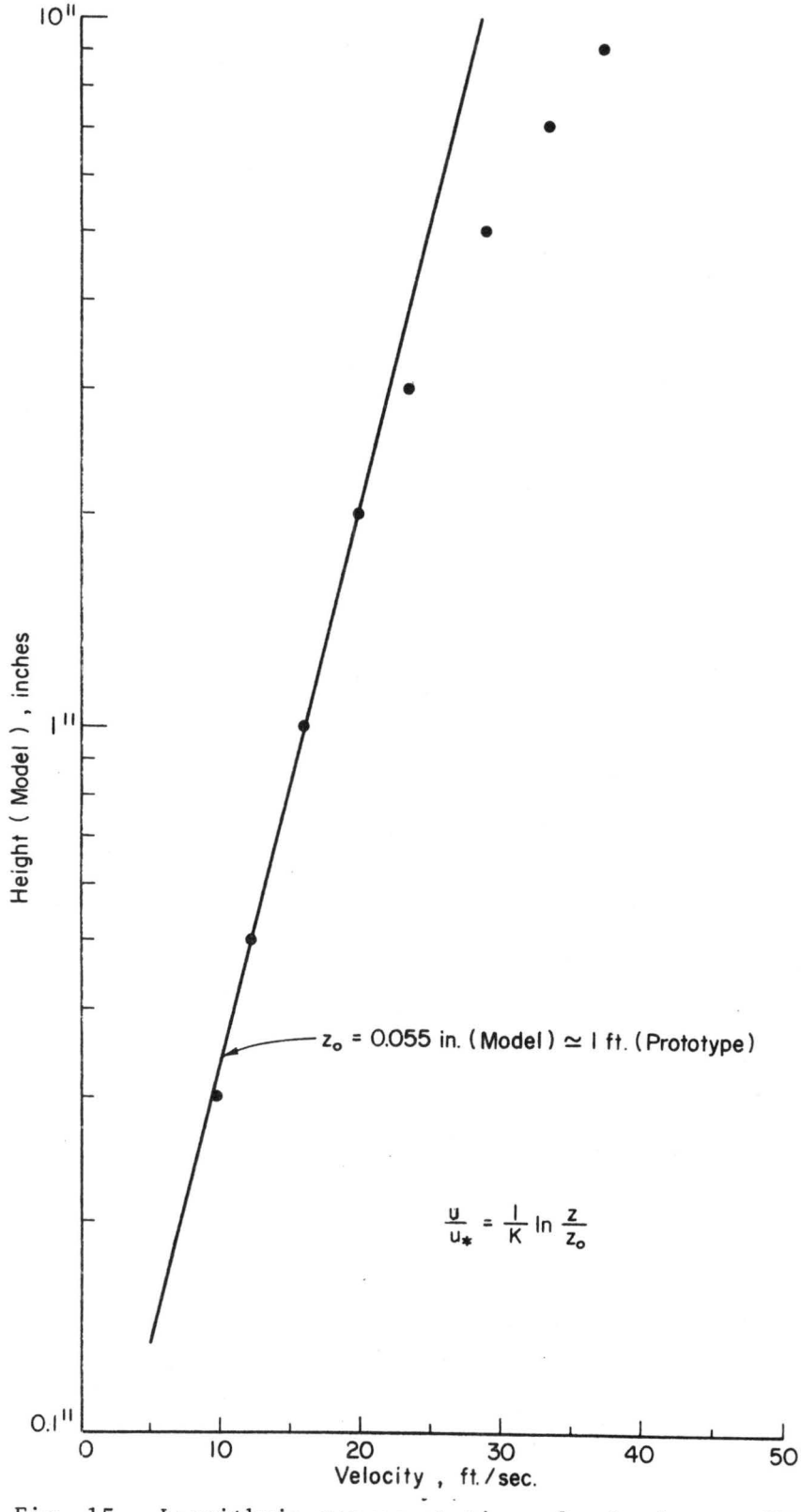

Fig. 15. Logrithmic representation of velocity profile.

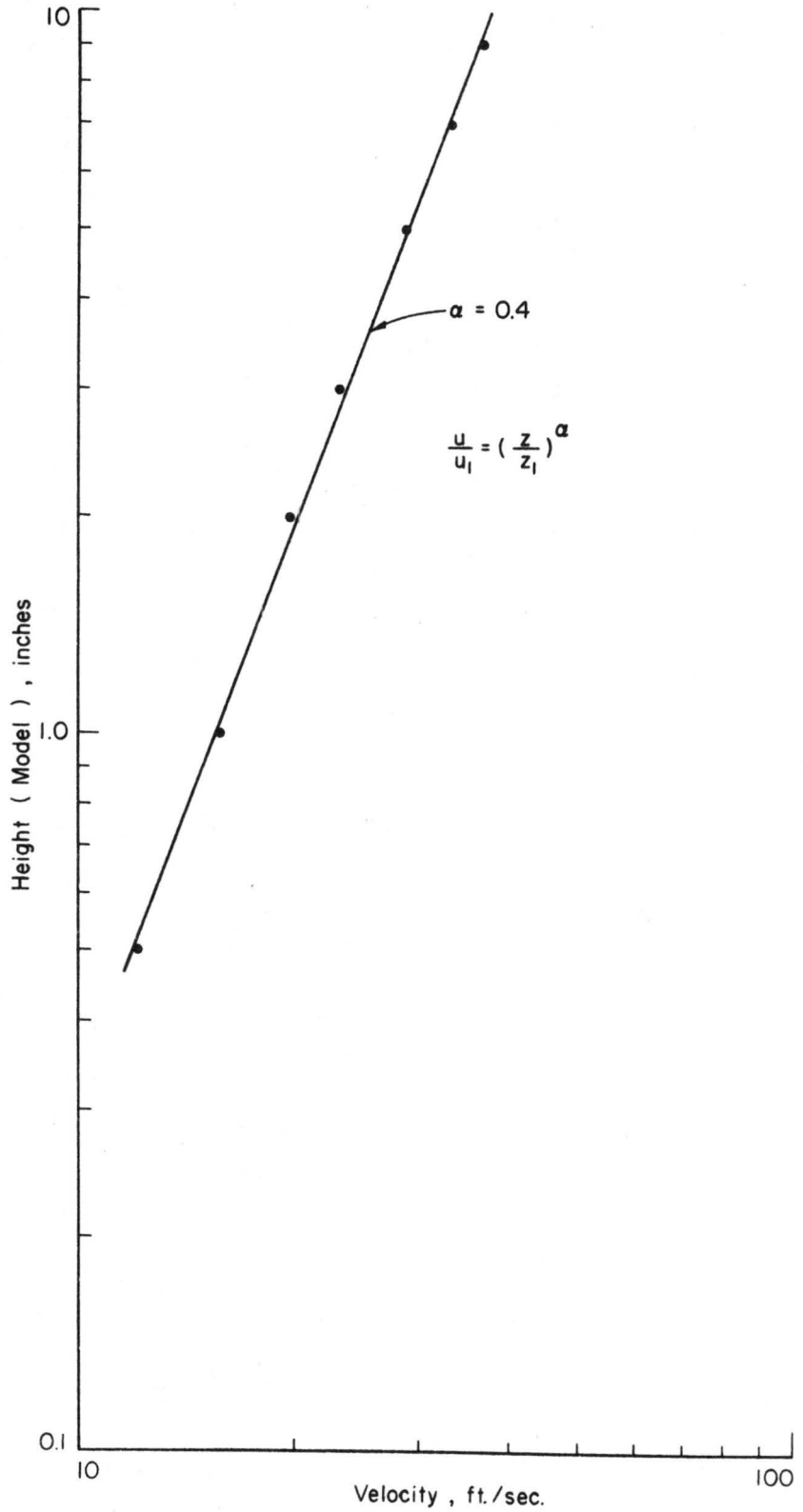

Fig. 16. Power-law representation of velocity profile.

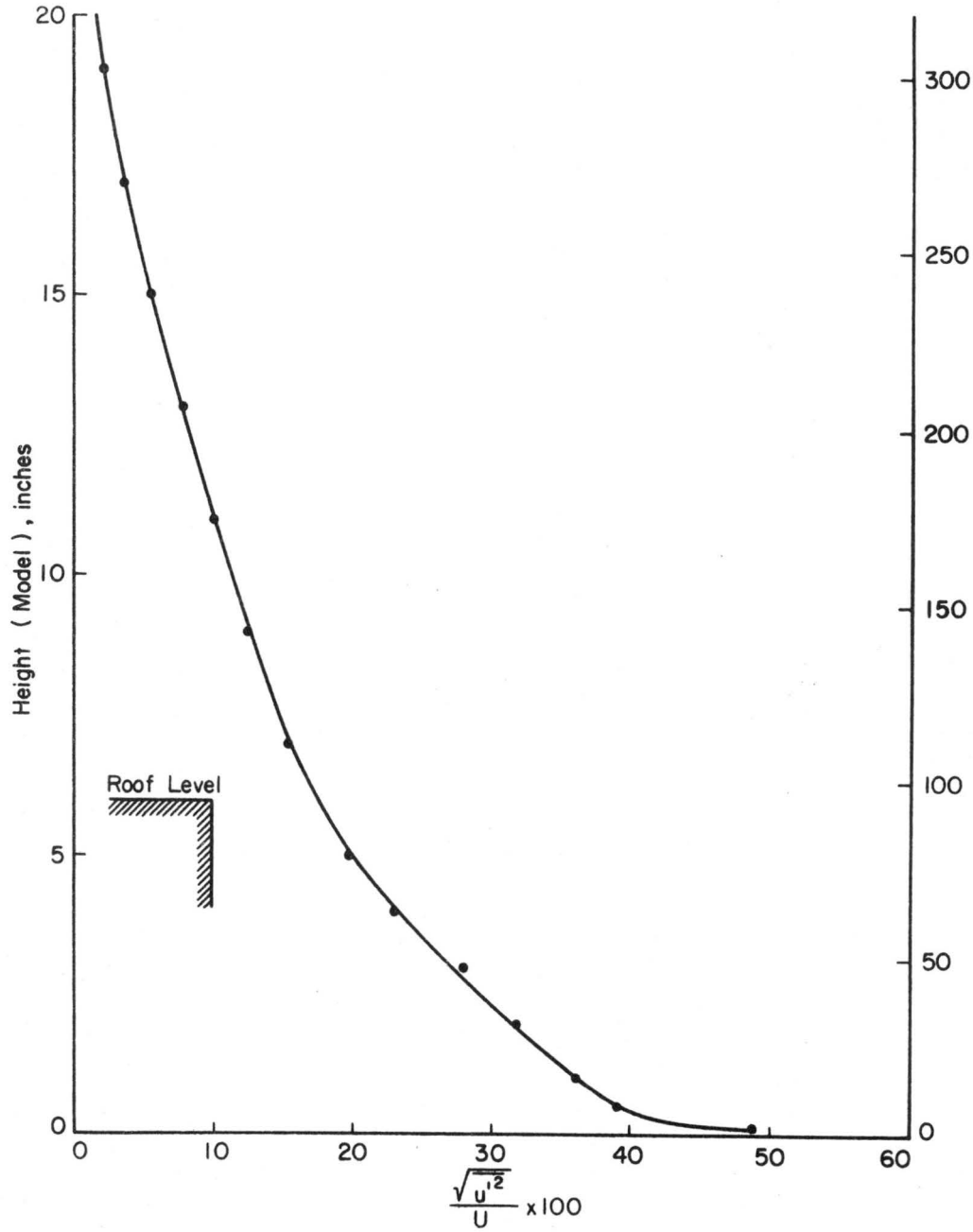

Fig. 17. Approach flow turbulence profile at a distance equivalent to 1000 ft upwind from Children's Hospital facility.

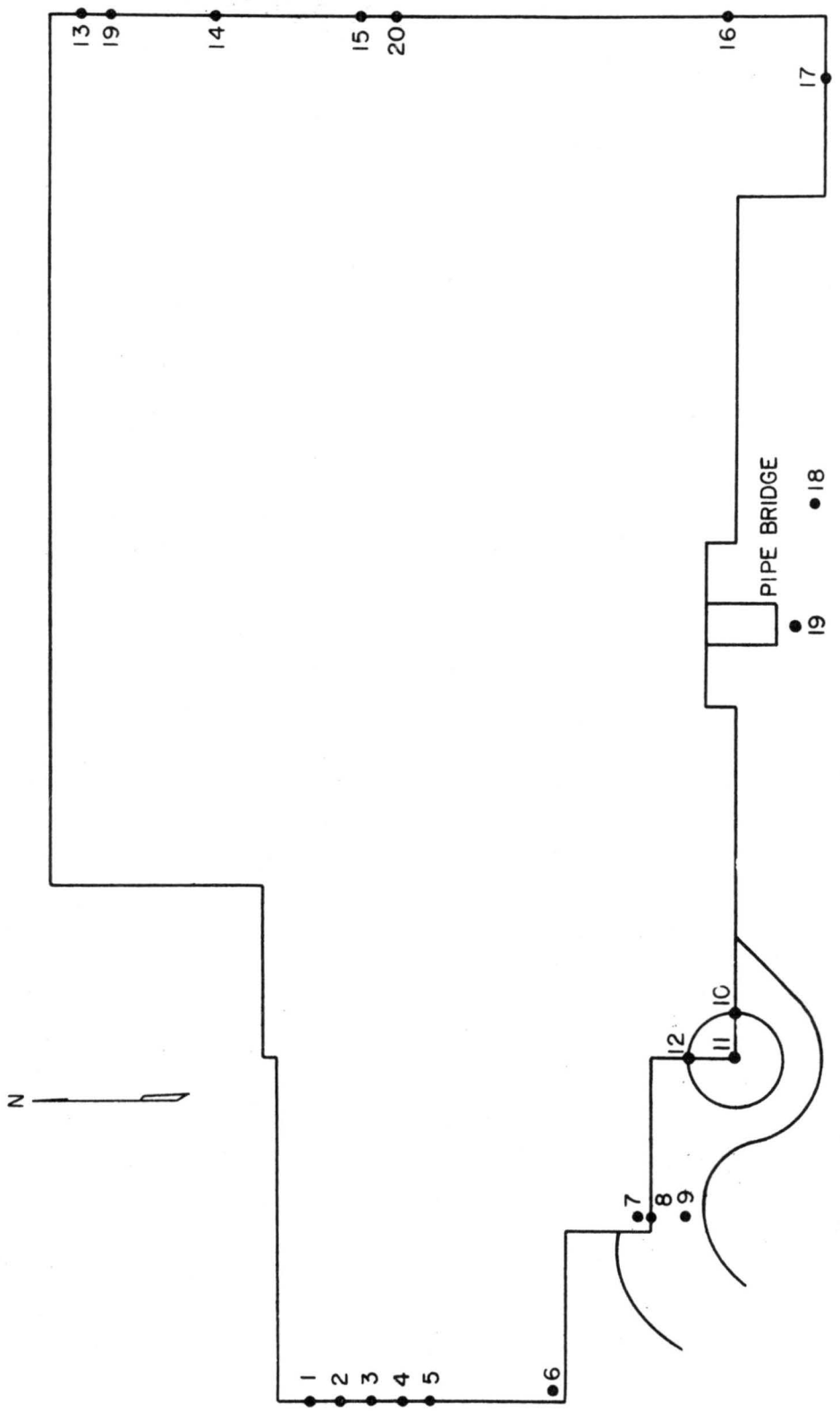

Fig. 18. Location of wind and turbulence measurements at level 'V-1'.

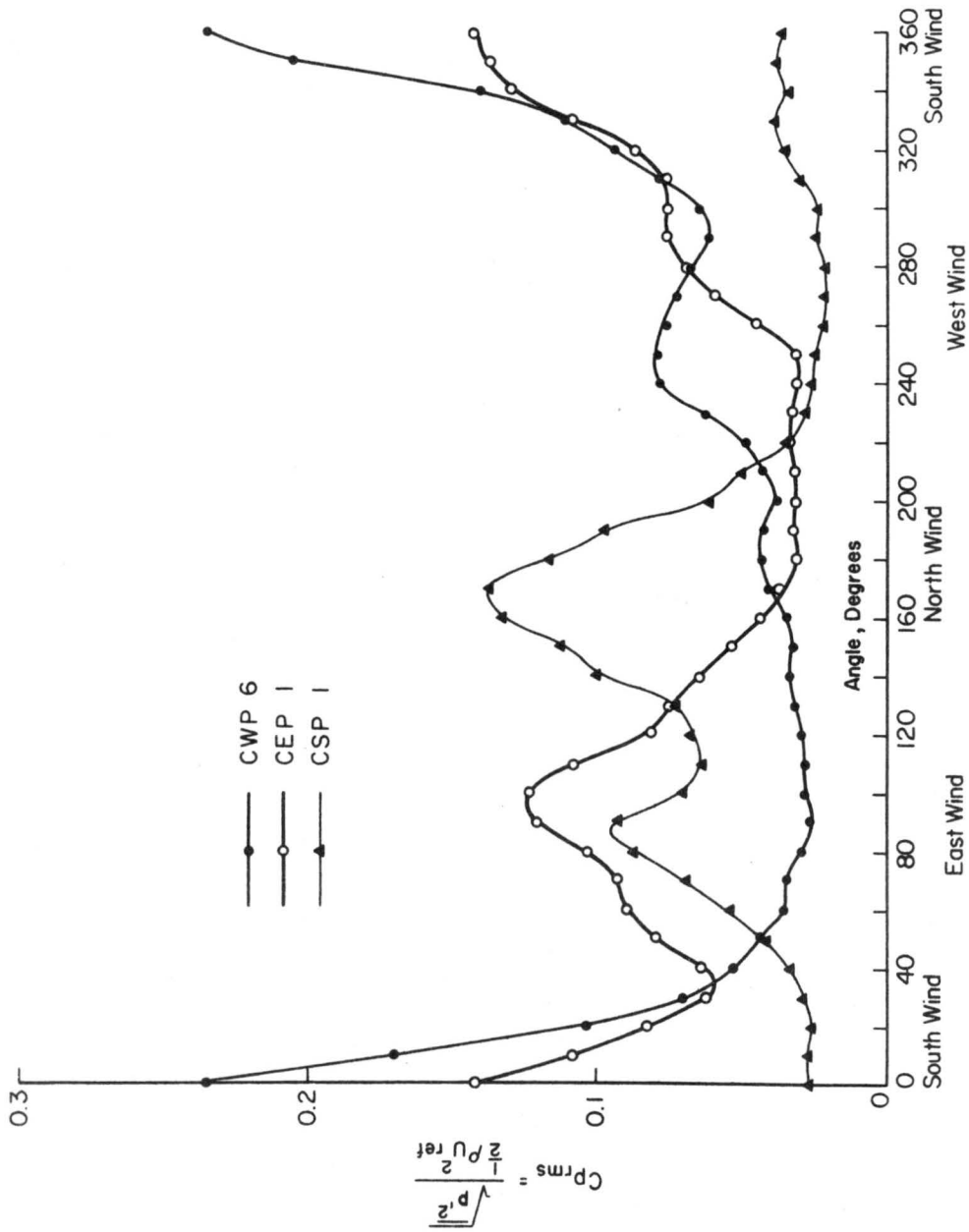

Fig. 19. Variation of pressure fluctuations with wind direction for selected pressure taps.

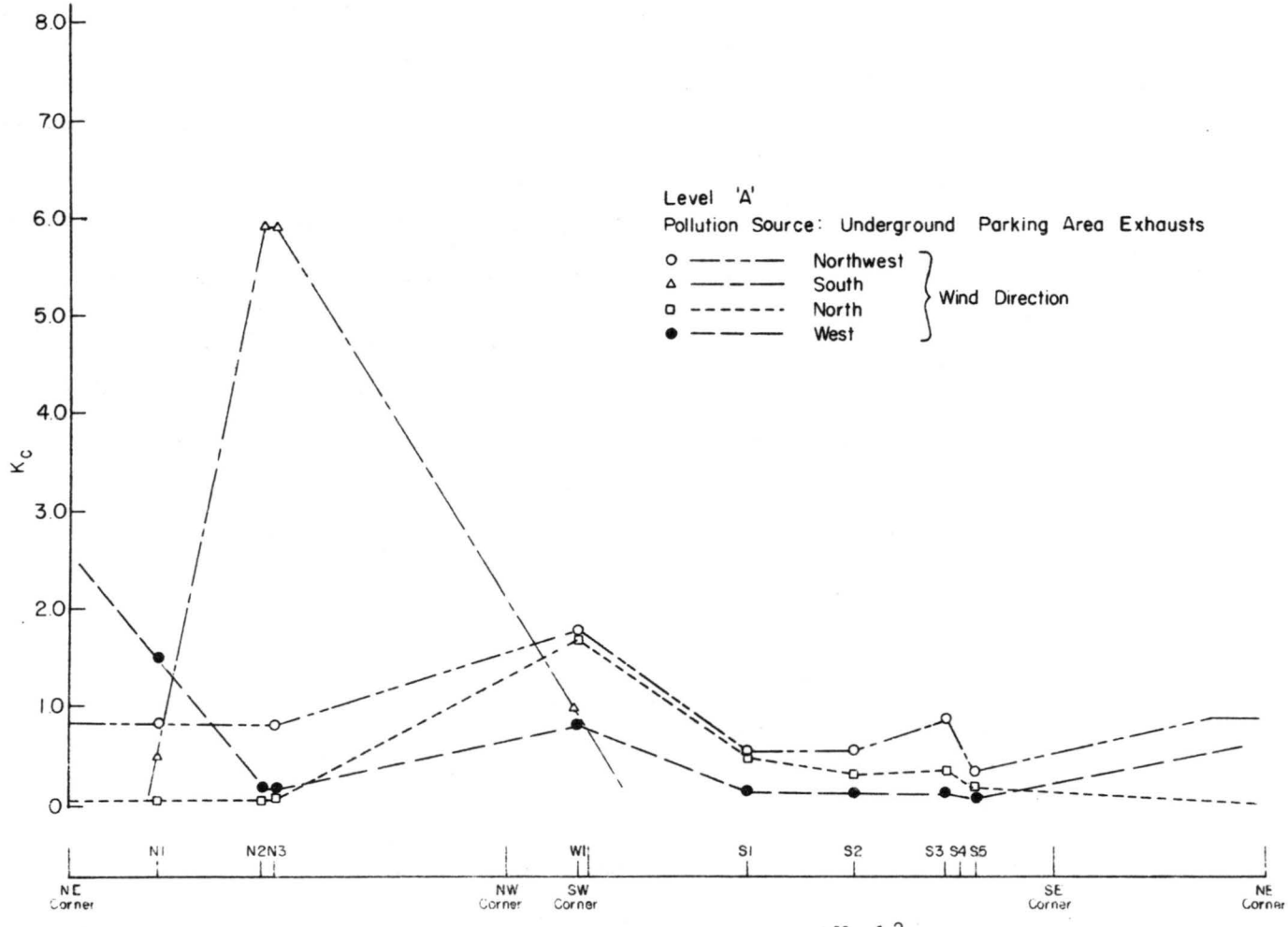

Fig. 20. Variation of non-dimensional concentration K_c (= $\frac{cU_h h^2}{Q}$) at level 'A' around the facility due to parking area exhausts for various wind directions.

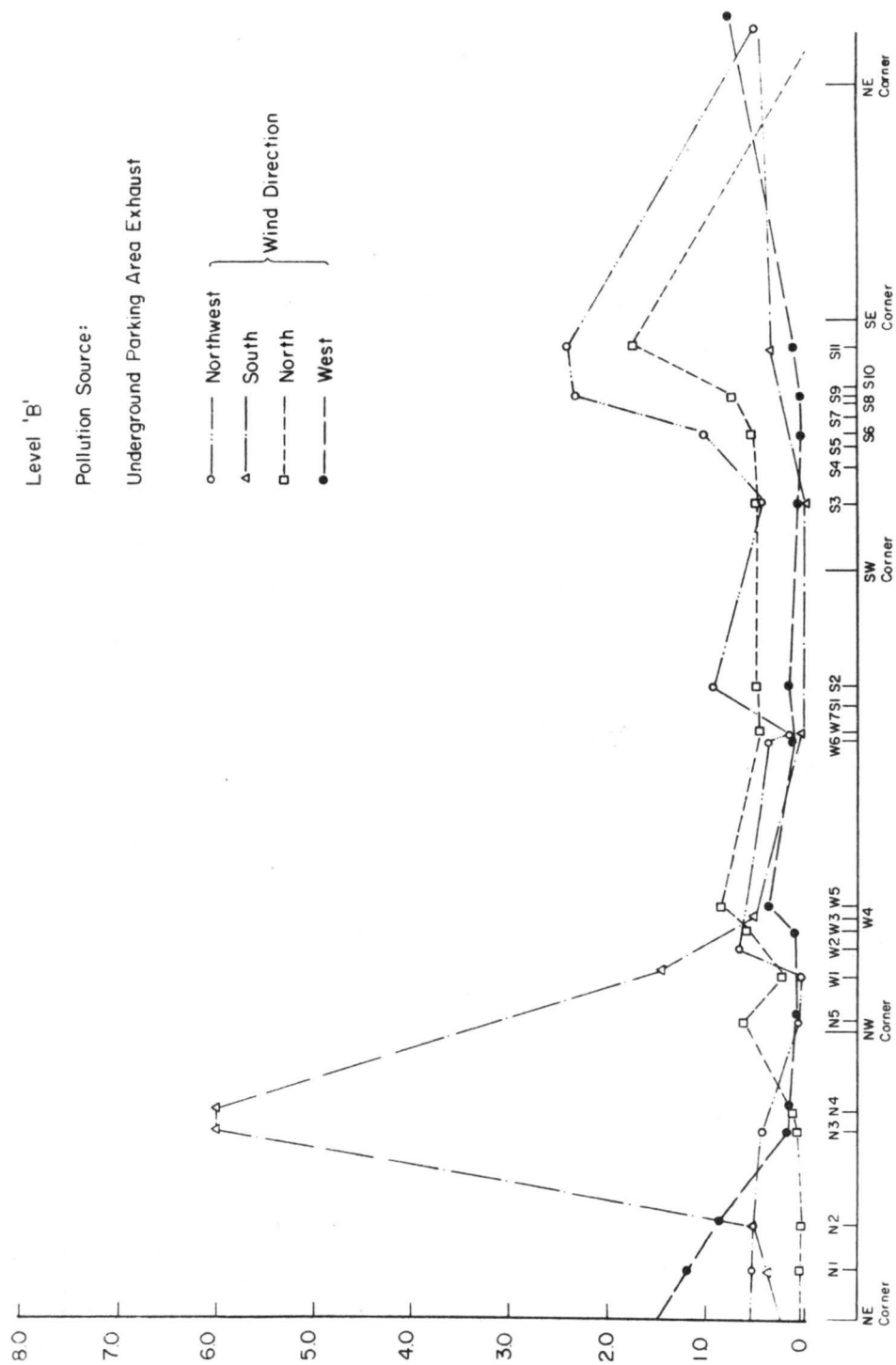

Fig. 21. Variation of non-dimensional concentration K_c (= $\frac{cU_h h^2}{Q}$) at level 'B' around the facility due to parking area exhausts for various wind directions.

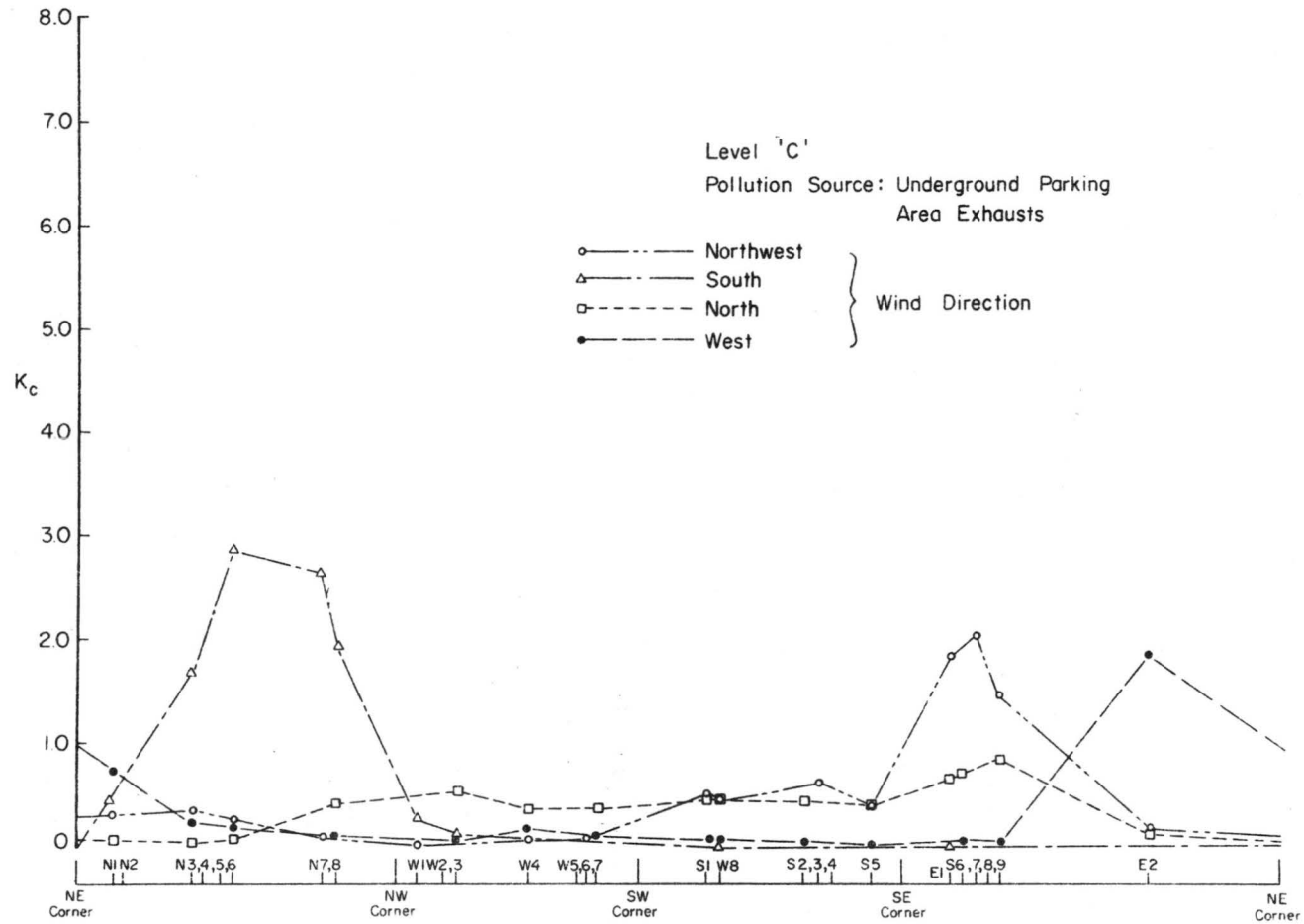

Fig. 22. Variation of non-dimensional concentration K_c (= $\frac{cU_h h^2}{Q}$) at level 'C' around the facility due to parking area exhausts for various wind directions.

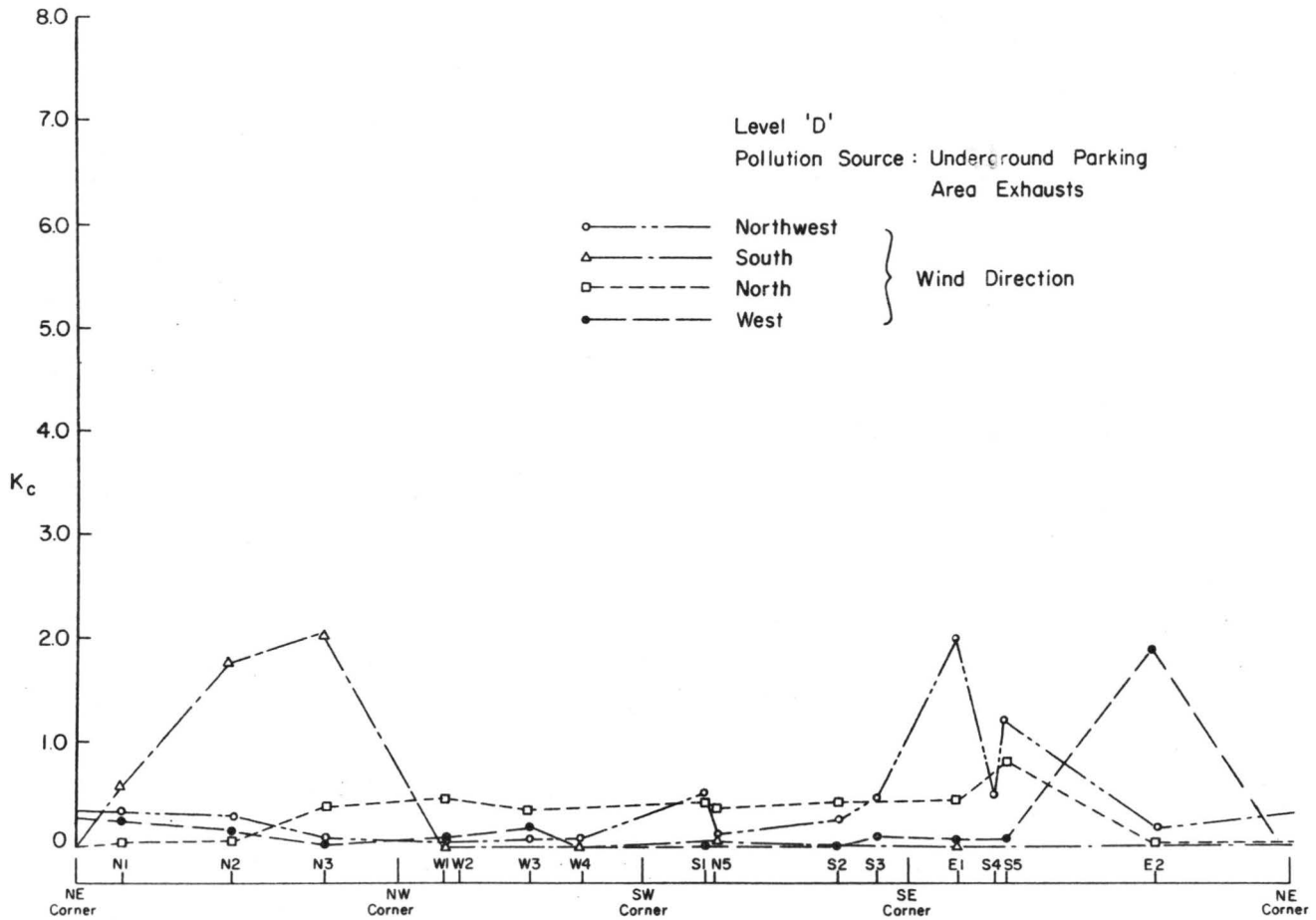

Fig. 23. Variation of non-dimensional concentration K_c ($= \frac{cU_h h^2}{Q}$) at level 'D' around the facility due to parking area exhausts for various wind directions.

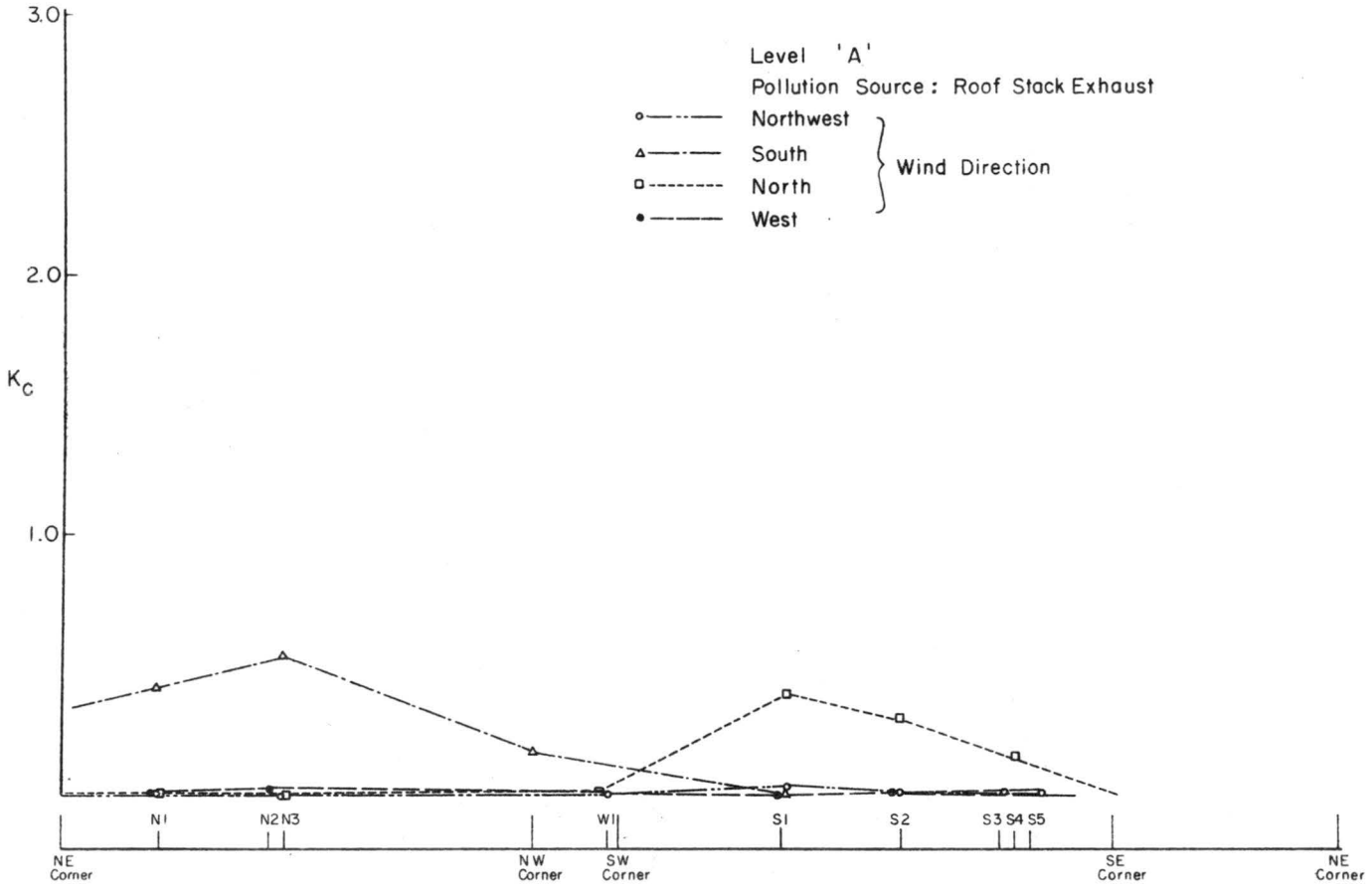

Fig. 24. Variation of non-dimensional concentration K_c (= $\frac{cU_h h^2}{Q}$) at level 'A' around the facility due to roof stack exhausts for various wind directions.

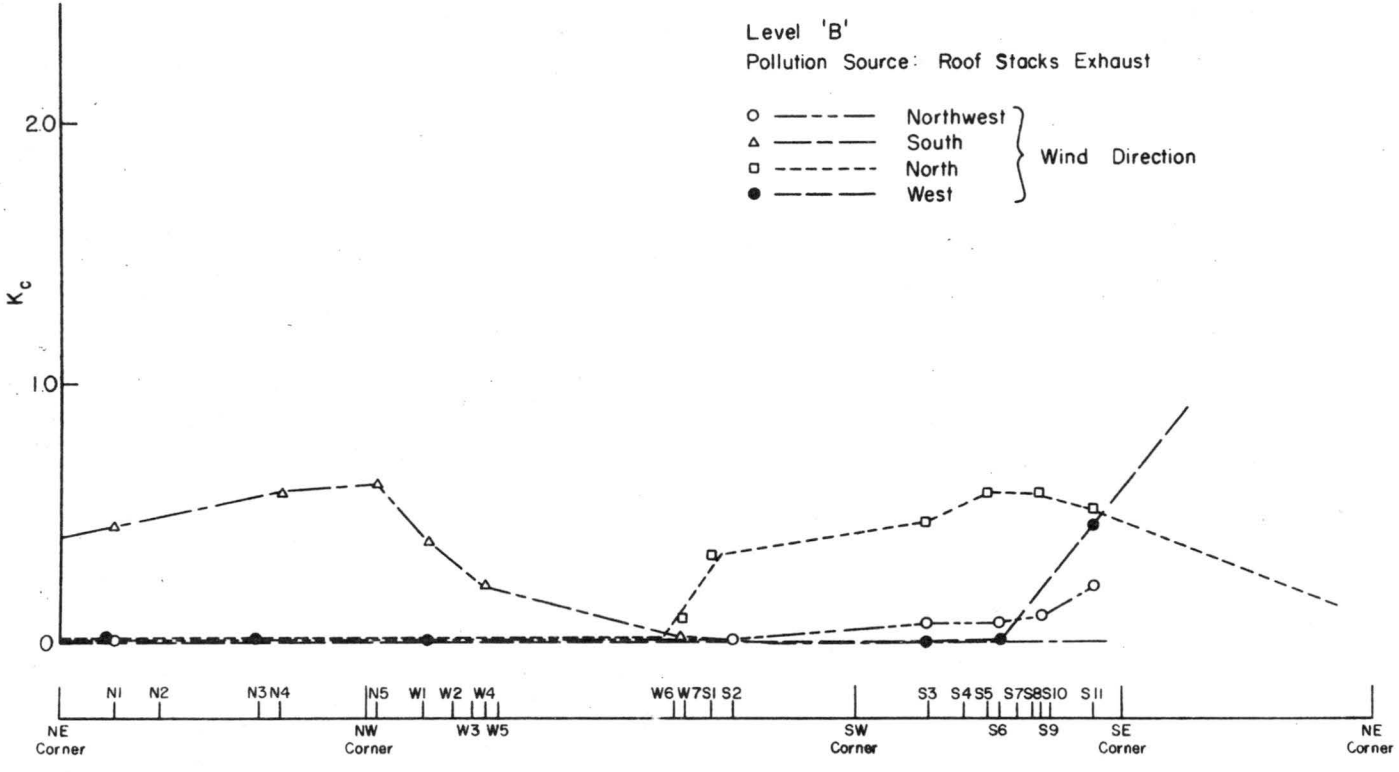

Fig. 25. Variation of non-dimensional concentration K_c (= $\frac{cU_h h^2}{Q}$) at level 'B' around the facility due to roof stack exhausts for various wind directions.

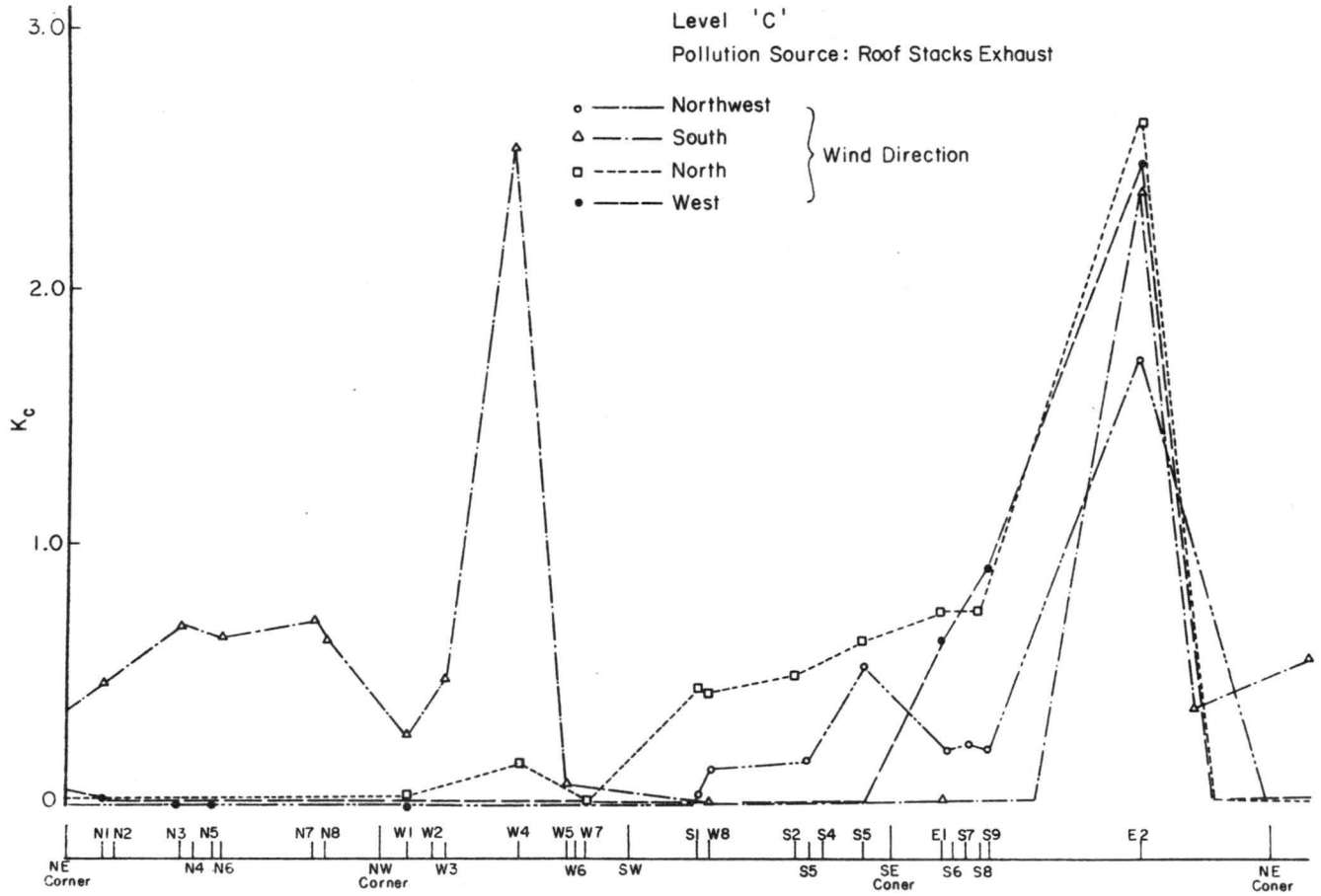

Fig. 26. Variation of non-dimensional concentration K_c ($= \frac{cU_h h^2}{Q}$) at level 'C' around the facility due to roof stack exhausts for various wind directions.

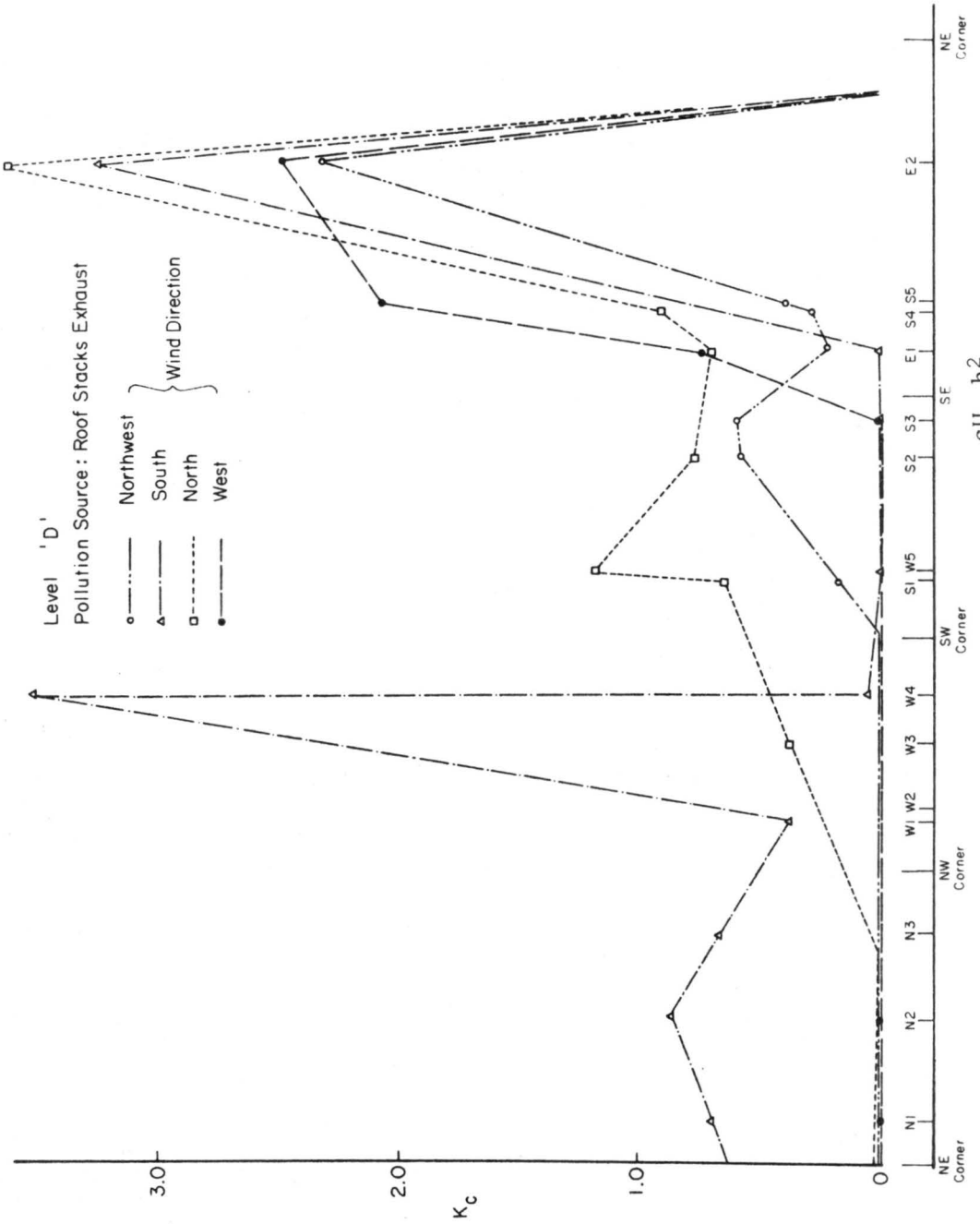

Fig. 27. Variation of non-dimensional concnetration K_c (= $\frac{cU_h h^2}{Q}$) at level 'D' around the facility due to roof stack exhausts for various wind directions.

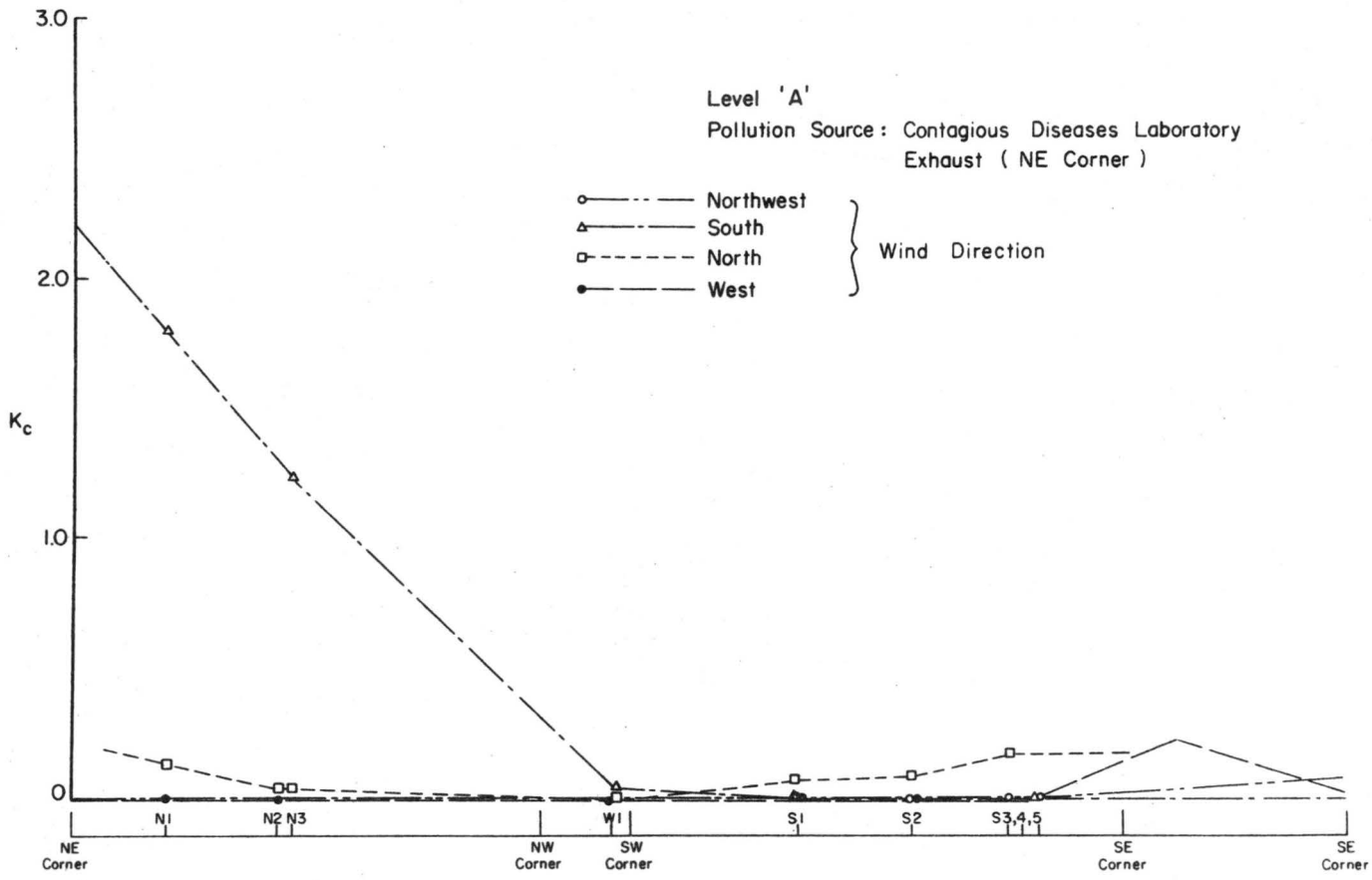

Fig. 28. Variation of non-dimensional concentration K_c (= $\frac{cU_h h^2}{Q}$) at level 'A' around the facility due to contagious diseases lab. (NE corner) for various wind directions.

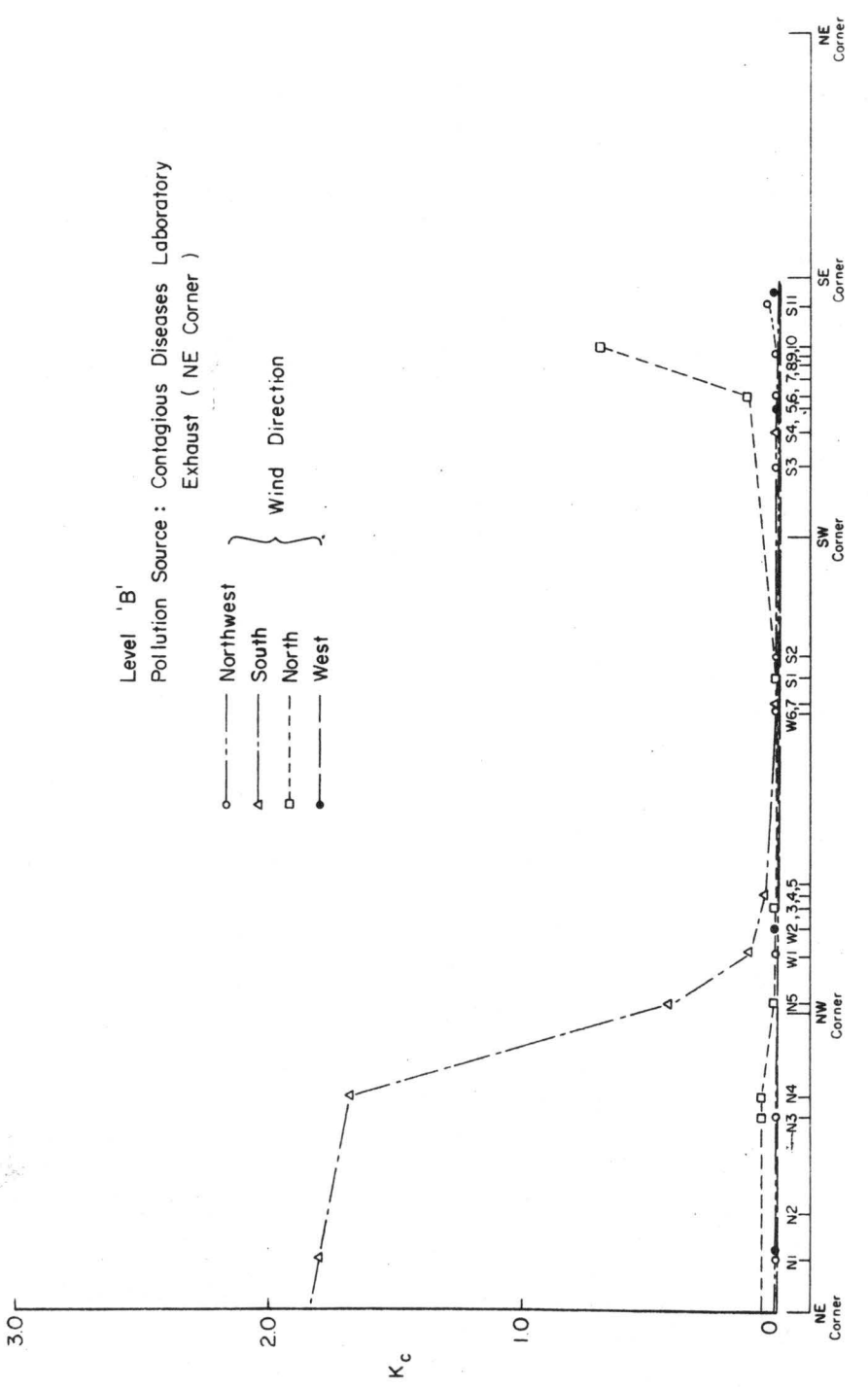

Fig. 29. Variation of non-dimensional concentration K_c (= $\frac{cU_h h^2}{Q}$) at level 'B' around the facility due to contagious diseases lab. (NE corner) for various wind directions.

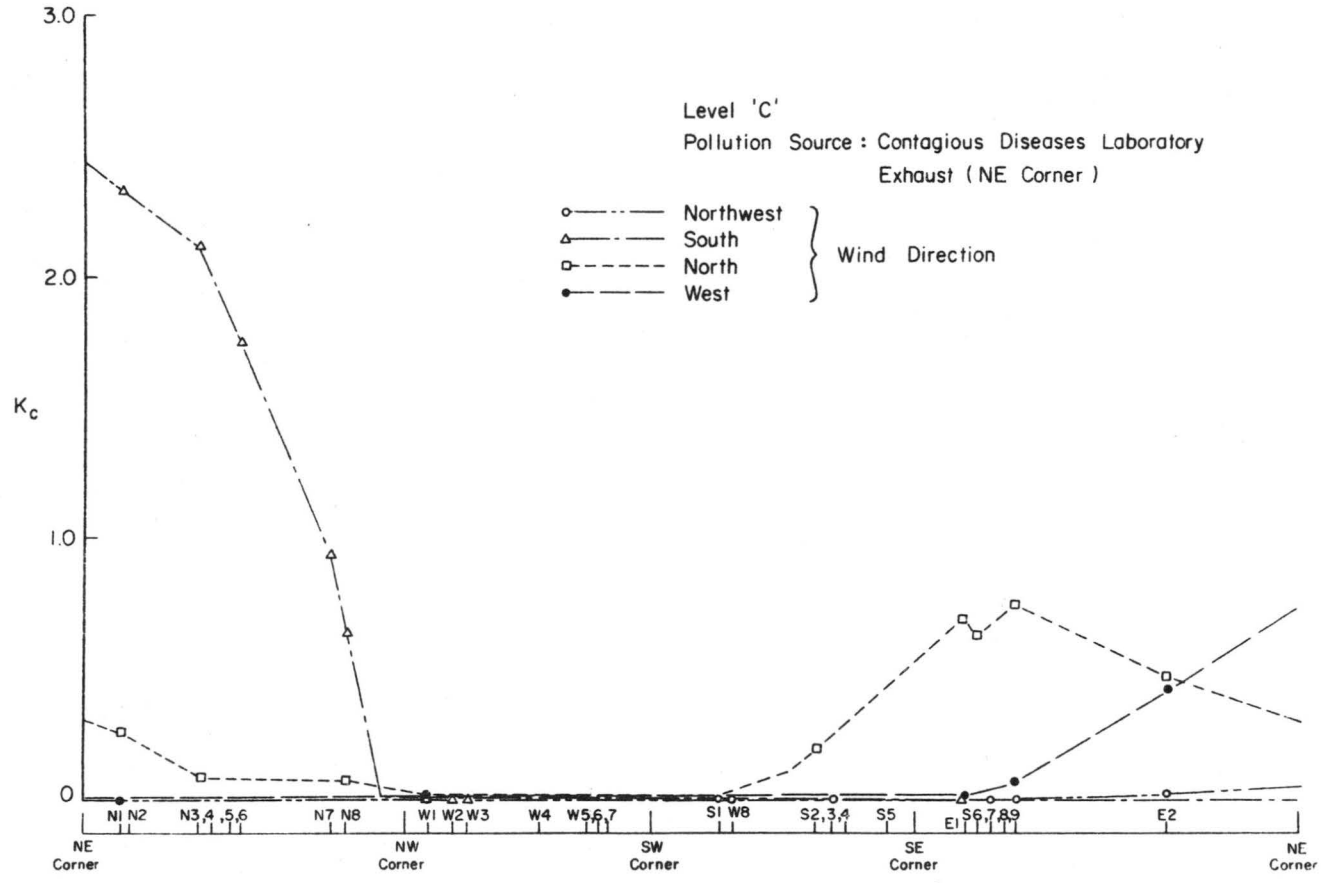

Fig. 30. Variation of non-dimensional concentration K_c ($= \frac{cU_h h^2}{Q}$) at level 'C' around the facility due to contagious diseases lab. (NE corner) for various wind directions.

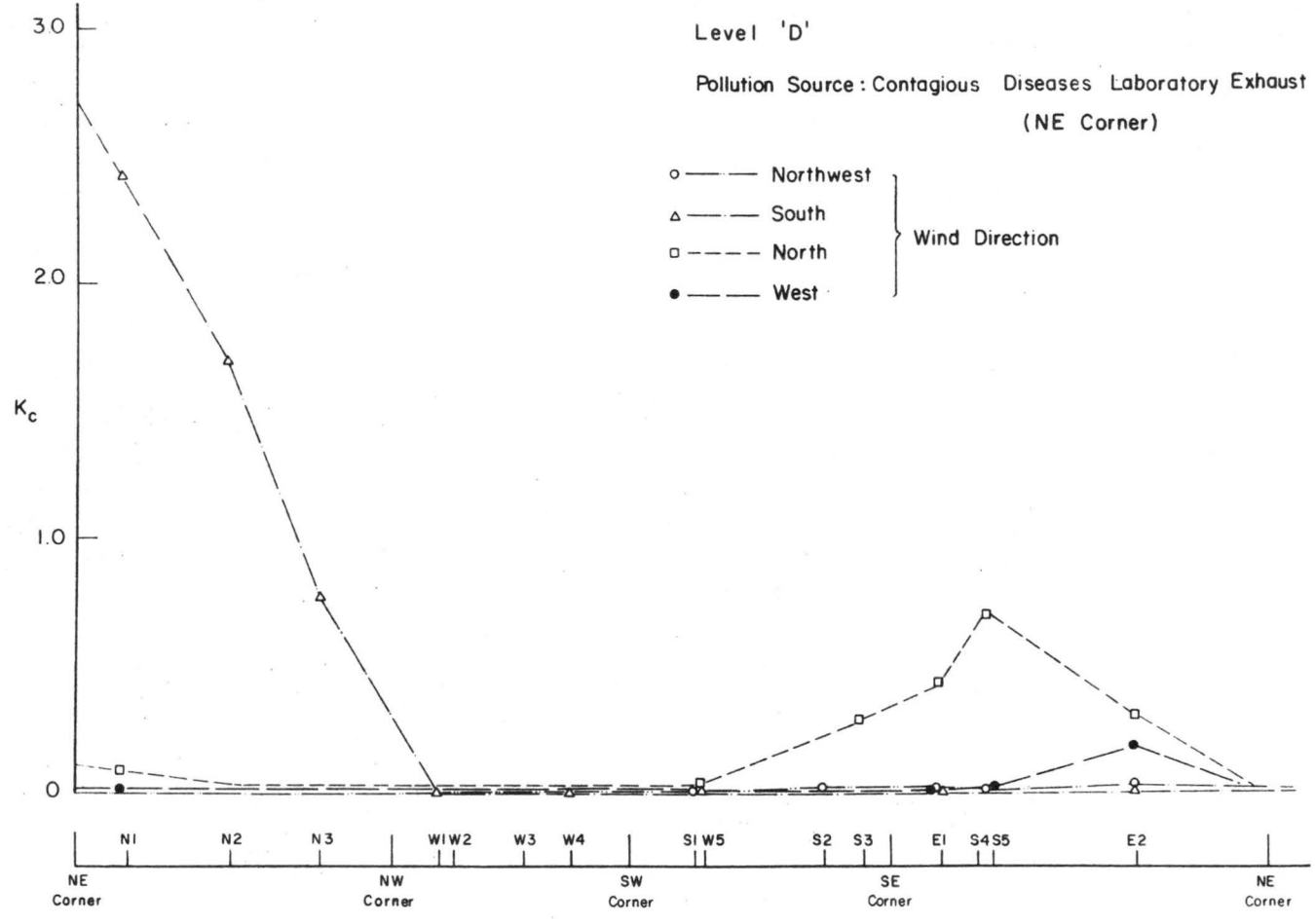

Fig. 31. Variation of non-dimensional concentration K_c ($= \frac{cU_h h^2}{Q}$) at level 'D' around the facility due to contagious diseases lab. (NE corner) for various wind directions.

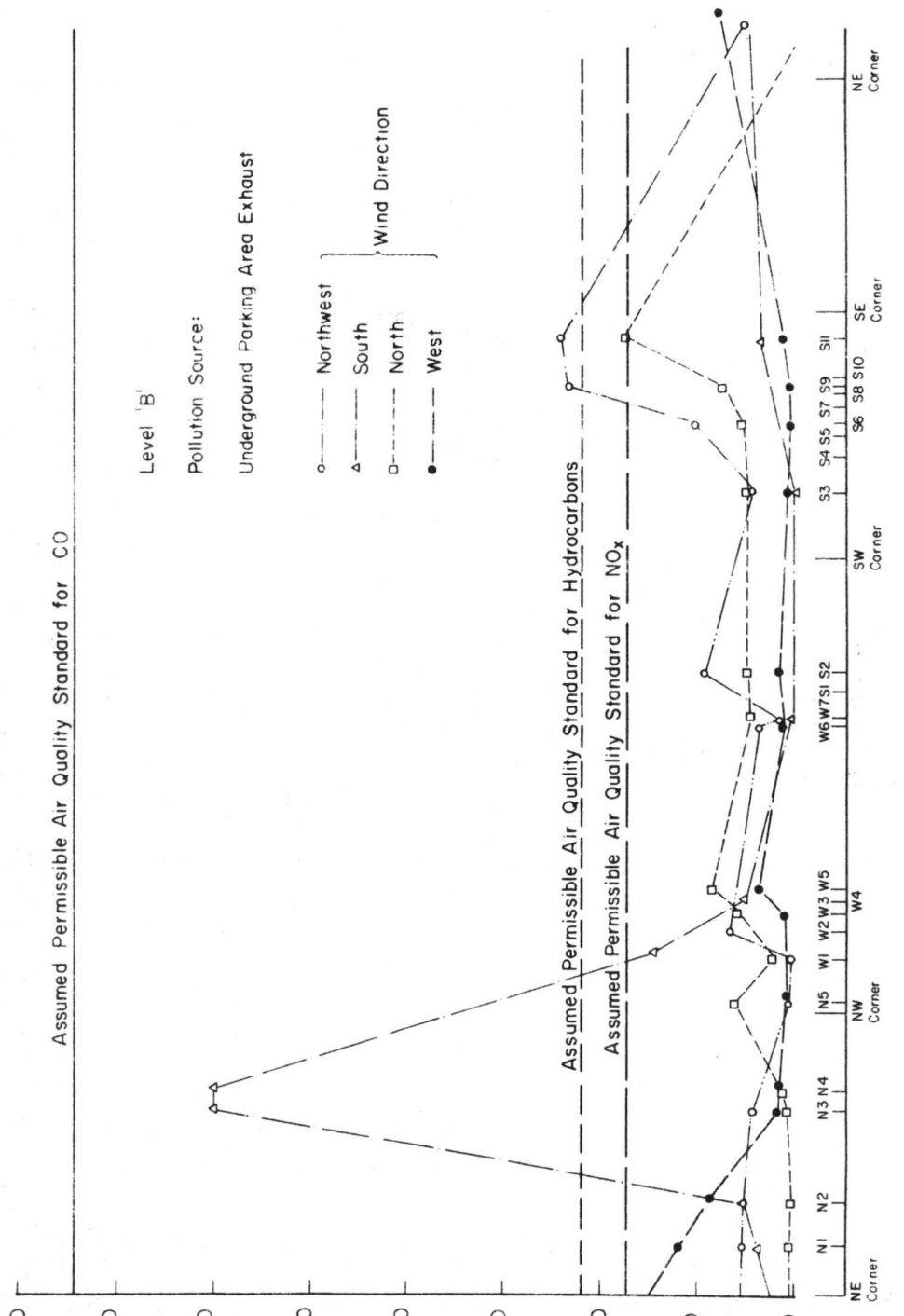

Fig. 33. Comparison of non-dimensional concentrations K_c (= $\frac{cU_h h^2}{Q}$) at level 'B' with the non-dimensional assumed permissible concentrations (reference wind 10 mph) of carbon monoxide, hydrocarbons and nitrogen oxides for parking area exhausts.

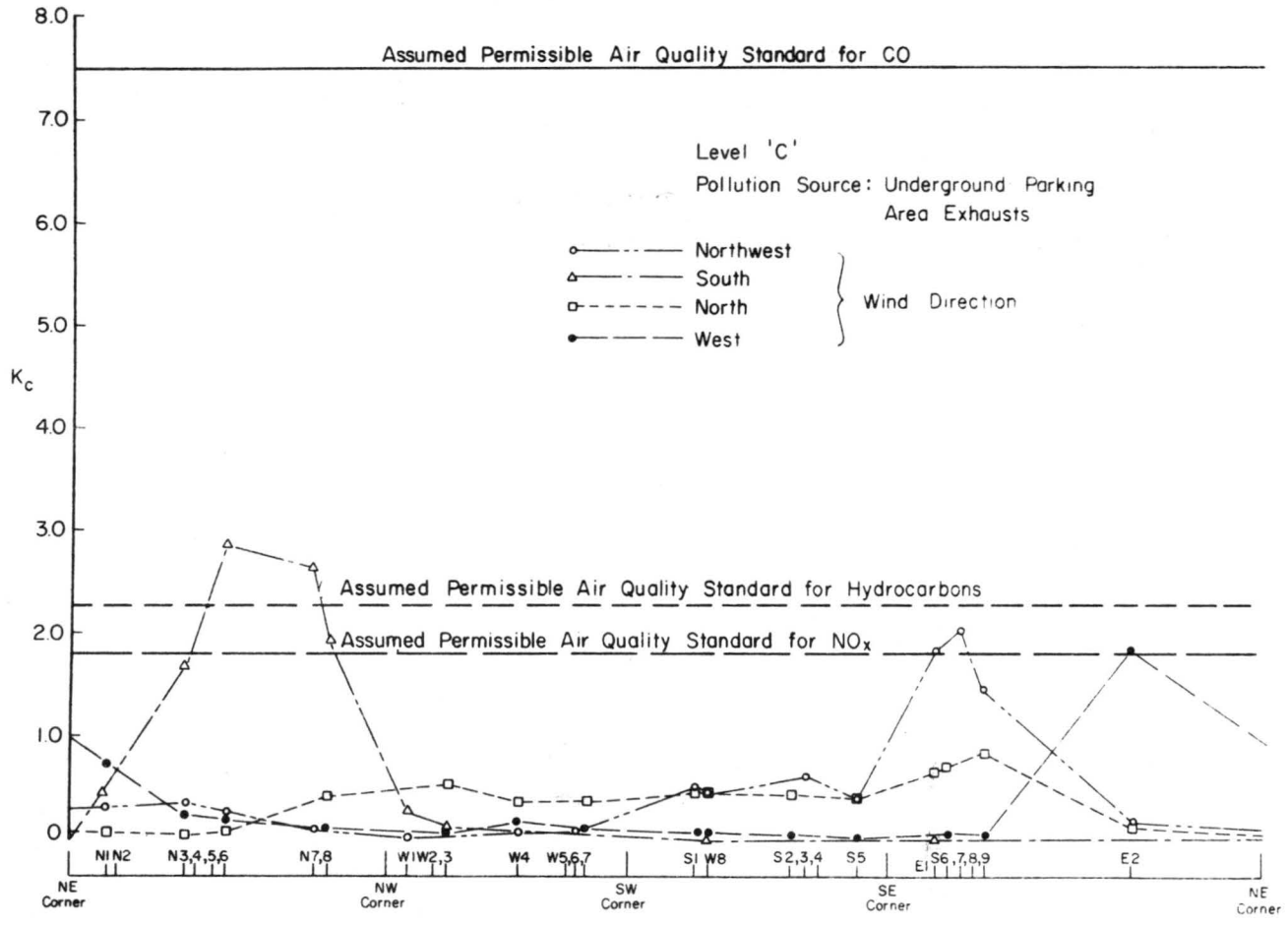

Fig. 34. Comparison of non-dimensional concentrations K_c (= $\frac{cU_h h^2}{Q}$) at level 'C' with the non-dimensional assumed permissible concentrations (reference wind 10 mph) of carbon monoxide, hydrocarbons and nitrogen oxides for parking area exhausts.

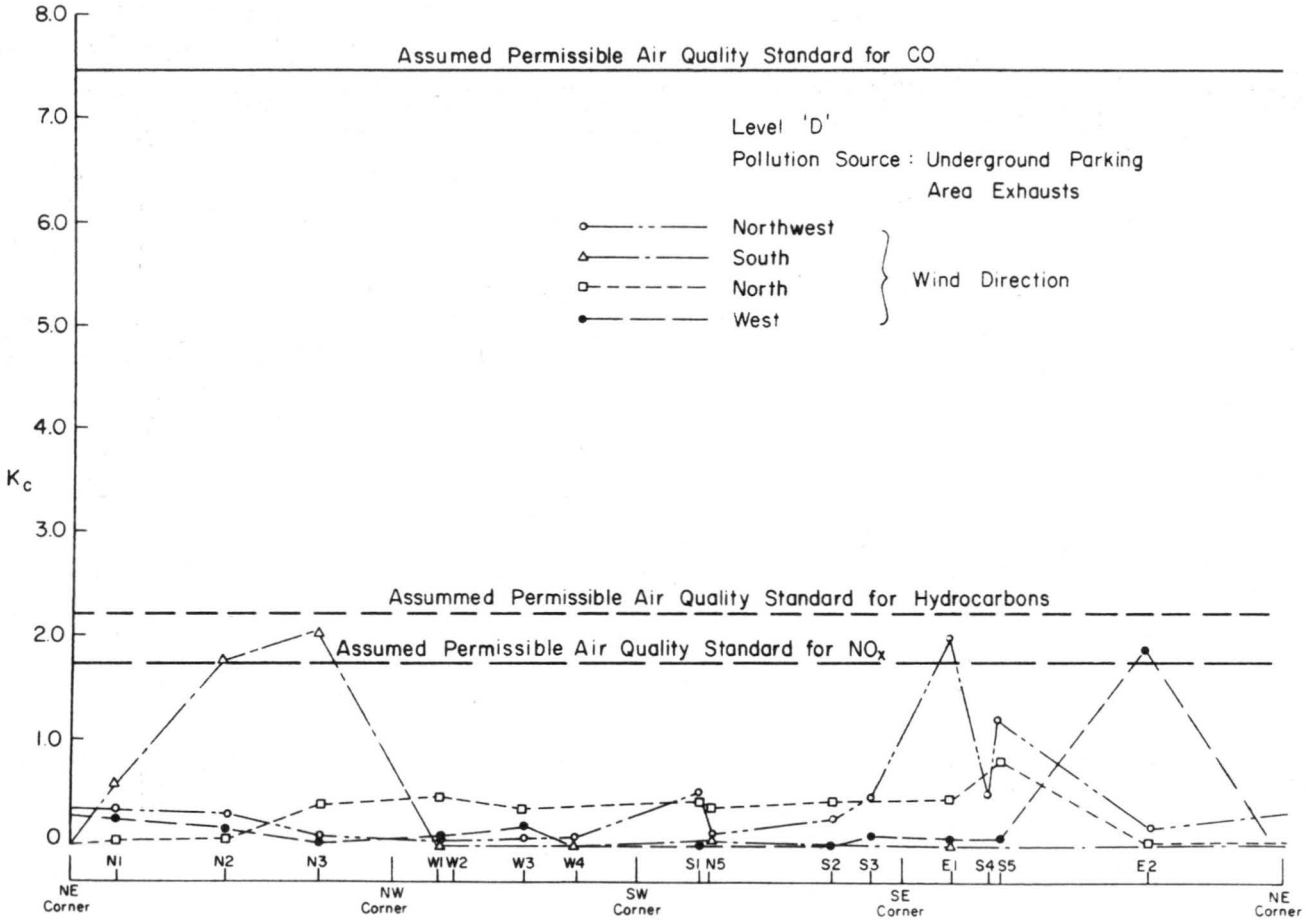

Fig. 35. Comparison of non-dimensional concentrations K_c ($= \frac{cU_h h^2}{Q}$) at level 'D' with the non-dimensional assumed permissible concentrations (reference wind 10 mph) of carbon monoxide, hydrocarbons and nitrogen oxides for parking area exhausts.